

## In search of the source of asteroid (101955) Bennu: Applications of the stochastic YORP model



William F. Bottke<sup>a,\*</sup>, David Vokrouhlický<sup>b</sup>, Kevin J. Walsh<sup>a</sup>, Marco Delbo<sup>c</sup>, Patrick Michel<sup>c</sup>, Dante S. Lauretta<sup>d</sup>, Humberto Campins<sup>e</sup>, Harold C. Connolly Jr.<sup>f,g,h</sup>, Daniel J. Scheeres<sup>i</sup>, Steven R. Chelsey<sup>j</sup>

<sup>a</sup>Southwest Research Institute and the Institute for the Science of Exploration Targets (ISET), 1050 Walnut St, Suite 300, Boulder, CO 80302, USA

<sup>b</sup>Institute of Astronomy, Charles University, Prague, V Holešovičkách 2, 180 00 Prague 8, Czech Republic

<sup>c</sup>University of Nice-Sophia Antipolis, CNRS, Côte d'Azur Observatory, France

<sup>d</sup>Lunar and Planetary Laboratory, University of Arizona, Tucson, AZ 85721, USA

<sup>e</sup>Physics Department, University of Central Florida, P.O. Box 162385, Orlando, FL 32816-2385, USA

<sup>f</sup>Dept. Physical Sciences, Kingsborough Community College of CUNY, 2001 Oriental Blvd., Brooklyn, NY 100235, USA

<sup>g</sup>Earth and Environmental Sciences, The Graduate Center of CUNY, 365 5th Ave., New York, NY 10016, USA

<sup>h</sup>Dept. Earth and Planetary Sciences, AMNH, Central Park West, New York, NY 10024, USA

<sup>i</sup>Department of Aerospace Engineering Sciences, Colorado Center for Astrodynamics Research, The University of Colorado at Boulder, 429 UCB, Boulder, CO 80309-0429, USA

<sup>j</sup>Jet Propulsion Laboratory, M/S 301-121, 4800 Oak Grove Dr., Pasadena, CA 91109, USA

### ARTICLE INFO

#### Article history:

Received 19 August 2014

Revised 24 September 2014

Accepted 24 September 2014

Available online 6 October 2014

#### Keywords:

Asteroids  
Asteroids, dynamics  
Near-Earth objects  
Celestial mechanics

### ABSTRACT

Asteroid (101955) Bennu, the target of NASA's OSIRIS-REx sample return mission, is a  $D \approx 0.5$  km diameter low albedo near-Earth object. It has a spectral signature consistent with primitive carbonaceous chondrites, and an orbit similar to that of the Earth. A plausible evolution scenario for Bennu is that it migrated inward across the inner main belt from a low albedo family by Yarkovsky thermal forces over many hundreds of Myr. Eventually, it entered a resonance that took it into the terrestrial planet region, where a combination of planetary encounters and resonances took it to its current orbit over a few Myr to tens of Myr. When it departed the main belt, Bennu probably had an eccentricity  $0.1 < e < 0.2$  and an inclination  $1^\circ < i < 6^\circ$ . Several low albedo families have the appropriate dynamical, color, albedo, and broad spectral characteristics to produce Bennu: Clarissa, Erigone, Eulalia, New Polana, and Sulamitis.

Here we used a suite of numerical simulations to determine the ages of the families above, how Bennu reached its current orbit, and the most probable source family for Bennu. Specifically, we tracked test Bennu-like asteroids evolving in semimajor axis by the coupled Yarkovsky/YORP effects, incorporating a new formalism for how YORP torques modify the spin vector evolution of small asteroids. Using results and insights provided by Statler (Statler, T.S. [2009], *Icarus* 202, 502–513), we assumed that modest shape changes to asteroids, produced by a variety of processes (e.g., crater formation, changes to asteroid rotational angular momentum by YORP), caused the test asteroids' spin rates, but not their obliquities, to undergo a random walk. This "stochastic YORP" mechanism slows down how often asteroids reach YORP endstates (i.e., spinning up so fast that the asteroid sheds mass, spinning down so much the asteroid enters into a tumbling rotation state). This new model allowed us to reproduce the semimajor axis distribution of observed family members from Clarissa, Erigone, Eulalia, New Polana, and Sulamitis. In the process, we derived model family formation ages of  $\sim 60$  Myr old,  $130 \pm 30$  Myr old,  $830_{-100}^{+370}$  Myr old,  $1400 \pm 150$  Myr old, and  $200 \pm 40$  Myr, respectively.

Next, using a Monte-Carlo code to track millions of test asteroids from each of the families above to main belt escape routes capable of producing Bennu-like orbits, we found the most likely parent families for Bennu are Eulalia and New Polana. On average, more than twice as many 0.5 km objects from the New Polana family reach Bennu's orbit as those from the Eulalia family. This corresponds to the New Polana and Eulalia families having a  $70_{-4}^{+8}\%$  and  $30_{-8}^{+4}\%$  probability of producing Bennu, respectively. Comparable runs to deduce the source of the Hayabusa 2 target, the low albedo 0.87 km diameter near-Earth object (162173) 1999 JU3, produced similar probabilities for both families. The former Marco-Polo-R target, the 1.9 km asteroid (175706) 1996 FG3, however, has a  $85_{-83}^{+4}\%$  probability of coming from the Eulalia family and a  $15_{-4}^{+83}\%$  probability of coming from the New Polana family. The reason for this switch is that 1996

\* Corresponding author.

E-mail address: [bottke@boulder.swri.edu](mailto:bottke@boulder.swri.edu) (W.F. Bottke).

FG3 may have been part of Yarkovsky/YORP-produced wave of like-sized bodies that is only now reaching the terrestrial planet region. We suggest that the top-like shape of Bennu is a byproduct of mass wasting and/or mass shedding events produced by YORP spin up during its long journey across the inner main belt.

© 2014 Elsevier Inc. All rights reserved.

## 1. Introduction

NASA's OSIRIS-REx (Origins Spectral Interpretation Resource Identification Security Regolith Explorer) mission is planning to visit and return a sample from near-Earth asteroid (101955) Bennu, (its provisional designation was 1999 RQ<sub>36</sub>; hereafter we will call it Bennu) (Lauretta et al., *in press*). Bennu is a low albedo  $D \approx 0.5$  km diameter B-class asteroid whose spectral signature is most consistent with primitive CI or CM carbonaceous chondrites (Clark et al., 2011; Nolan et al., 2013). The goal is for OSIRIS-REx to bring back pristine materials and organic compounds that can help us better understand the characteristics of planetesimals that may have been the building blocks for life. Consider that while km- and sub-km-sized near-Earth objects (NEOs) with C-complex taxonomy and low albedos comprise about a fourth to a third of all NEOs (Stuart and Binzel, 2004; Mainzer et al., 2012), carbonaceous chondrite meteorites only provide <3% of all meteorite falls (Burbine et al., 2002). This suggests that many CI and CM meteorites fail to survive passage through Earth's atmosphere. Even those that do make it to the ground are quickly contaminated by terrestrial organics and volatiles. Hence, by returning samples directly from Bennu's regolith, OSIRIS-REx will avoid contamination while gleaning insights into the kinds of primordial volatiles and organic compounds delivered to Earth early in its history. With its Earth-like orbit, Bennu is accessible to the OSIRIS-REx spacecraft on a low velocity trajectory, and thus is a superb candidate for sample return.

To maximize the OSIRIS-REx science return, it is crucial to understand as much as possible the origin and evolution of Bennu and its parent body. There is much we do not know. For example, it is likely that Bennu's parent body spent most of its life in the main asteroid belt, but we cannot yet say whether it was indigenous to the main belt region (e.g., Bottke et al., 2006b; Bottke and Asphaug, 2013; Levison et al., 2009; Walsh et al., 2011). Bennu's parent body may have also experienced a wide range of physical processes, such as thermal metamorphism, aqueous alteration, and impact heating. Many of these effects have potentially left their mark on Bennu material. By returning samples from Bennu, analyzing them, and then asking the best possible questions within a plausible evolutionary framework for Bennu, we hope to learn much about how planetesimals, small body reservoirs like the asteroid belt, and the planets reached their current state.

Goals for this analysis would be to (i) understand the precise formation mechanism for Bennu's parent body, (ii) glean insights into the history of the parent body over the last 4.5 Gyr of Solar System history, (iii) probe when Bennu, or its immediate precursor, formed as a collisional byproduct of an impact event on its parent body, and (iv) constrain the evolution of Bennu from its original orbit in the main belt all the way to its current orbit near Earth. A key starting point for all of this is to determine where Bennu came from in main asteroid belt, how long it took to get from this location to its observed orbit, and what likely happened to it en route.

### 1.1. A conceptual model of Bennu's origin and evolution

In broad strokes, using what we have learned about asteroid evolution over the past several decades, we can already construct

a reasonable scenario describing how Bennu reached its current orbit. Bennu probably started its life as part of a much larger body. This parent body was created by planetesimal formation mechanisms that may have involved the turbulent concentration of very small bodies in the primordial solar nebula (e.g., Johansen et al., 2007, 2012; Cuzzi et al., 2010). Insights into this process indicate Bennu's parent body probably had a diameter  $D > 100$  km when it was born (Morbidelli et al., 2009, though see Weidenschilling, 2011 for a contrasting view). The formation location could have been the main asteroid belt, but it may also have been another region altogether (e.g., the outer Solar System beyond Jupiter; Levison et al., 2009; Walsh et al., 2011; Bottke et al., 2006b; Bottke and Asphaug, 2013). If the latter is true, dynamical processes implanted the parent body within the main belt within the first few hundreds of Myr of Solar System history. Once formed, the parent body would have experienced early thermal evolution by the decay of radiogenic nuclides (e.g., McSween et al., 2002), while its surface would have been battered by impacts for billions of years of cratering events (e.g., Bottke et al., 2005a,b).

The portion of Bennu's story investigated in this paper starts when Bennu's parent body experienced a large cratering event or, more likely, a catastrophic disruption event. This collision would have created enormous numbers of fragments near the impact site, some which were Bennu-sized. We refer to the clustered proper semimajor axes  $a$ , eccentricities  $e$ , and inclinations  $i$  of the bodies as an asteroid family (see review by Knežević et al. (2002)).

Once created, Bennu, or perhaps a somewhat larger precursor, began to undergo dynamical evolution via the non-gravitational forces referred to as the Yarkovsky and Yarkovsky–O'Keefe–Radzievskii–Paddack (YORP) effects (Rubincam, 2000; see Bottke et al., 2002b, 2006a; Vokrouhlický and Bottke, 2012 for reviews). The Yarkovsky effect describes a small force that affects the orbital motion of  $D < 40$  km bodies. It is caused by sunlight; when these bodies heat up in the Sun, they eventually re-radiate the energy away as heat, which in turn creates a tiny thrust. This recoil acceleration is much weaker than solar and planetary gravitational forces, but it can produce substantial secular semimajor axis changes over timescales ranging from many millions to billions of years. The same physical phenomenon also creates a thermal torque that, complemented by a torque produced by scattered sunlight, can modify the rotation rates and obliquities of small bodies as well. This rotational variant has been coined the YORP effect (Rubincam, 2000). During the past decade or so, the Yarkovsky and YORP effects have been used to explore and potentially resolve a number of unsolved mysteries involving asteroids and meteoroids.

The coupled Yarkovsky and YORP effects likely modified Bennu's spin axis or its precursor to a value approaching  $180^\circ$ , the same value it has today. This allowed Bennu or its precursor to drift inward by the Yarkovsky effect far enough to reach a dynamical resonance capable of pushing it out of the main belt and onto a terrestrial planet-crossing orbit. If Bennu or its precursor had a high enough eccentricity within the main belt, and the right initial orbit, it could have also drifted directly onto a Mars-crossing orbit by the Yarkovsky effect. From there, a combination of planetary close encounters and resonances would have moved it to where we see it now, namely on a very Earth-like orbit.

En route, Bennu's precursors may have disrupted one or more times by collisions or by mass-shedding via YORP spin up, enough to take it to its current size. This kind of family-wide evolution is called a "collisional cascade"; family members fragment and create daughter products, with the entire ensemble gradually spreading its way across the main belt. In this fashion, families may provide fresh debris to main belt escape hatches long after the original parent body disrupted. Alternatively, Bennu might have always been near its current size, and it potentially avoided all meaningful collisions. In this paper, we model the latter scenario because it is the most tractable given our current knowledge and modeling abilities.

## 1.2. Previous work on the origin and dynamical evolution of Bennu

Previous work on the origin of Bennu has come from [Campins et al. \(2010\)](#). Using existing dynamical models of near-Earth object (NEO) evolution ([Bottke et al., 2002a](#)), insights on how asteroid families evolve by the Yarkovsky and YORP effects (see [Bottke et al., 2006b](#)), color data from the Sloan Digital Sky Survey (SDSS; [Parker et al., 2008](#)), and albedo/spectroscopy data of both Bennu and very low albedo families in the inner main belt, they concluded that Bennu probably came from the Polana family, an B-type inner main belt asteroid family residing at low inclinations. Its largest remnant has long been thought to be (142) Polana (semimajor axis  $a \approx 2.41$  AU). Until recently, it has been an enormous challenge to decipher the complicated Nysa–Polana cluster of asteroids. This region is dominated by overlapping swarms of asteroids, with SDSS data suggesting that an S-complex cluster (often called the Nysa family, though some argue (878) Mildred is a better candidate to be this family's largest remnant; [Cellino et al., 2001](#)) and C-complex cluster (referred to as the Polana family) overlap one another. Additional studies have revealed smaller clusters in the same zone ([Dykhuis, 2014](#), personal communication). All of these clusters are remnants of distinct breakup events taking place in the same part of space. The pioneering aspect of [Campins et al. \(2010\)](#) was their recognition that SDSS data was sufficient to distinguish a considerable portion of the Polana family from other clusters in the region.

The spectra and albedos of Bennu and Polana family members were similar enough to one another that [Campins et al. \(2010\)](#) argued they might be a match. By extrapolating from the Yarkovsky evolution trends of Polana's smaller members, they suggested Bennu-sized bodies had probably reached the  $\nu_6$  secular resonance located along the inner edge of the main belt. This was highly favorable to their scenario because low inclination Polana members entering the  $\nu_6$  resonance had a high likelihood of being delivered to Bennu-like orbits (e.g., [Bottke et al., 2002a](#)). These results, when combined with a lack of obvious alternative family sources, suggested to [Campins et al. \(2010\)](#) that the Polana family was the source of Bennu.

The straightforward story of [Campins et al. \(2010\)](#), however, has been modified by the results of [Walsh et al. \(2013\)](#). Using albedo data from the Wide-field Infrared Survey Explorer (WISE) mission ([Masiero et al., 2011, 2013](#)), combined with asteroid proper orbital elements, they found that (142) Polana is probably not a member of the Polana family. Instead, [Walsh et al. \(2013\)](#) deduced that a more likely largest remnant for this family was (495) Eulalia, located at 2.487 AU. Accordingly, the Eulalia family replaces the Polana family designation. Moreover, it appears the Eulalia family disrupted on the very brink of the powerful 3:1 mean motion resonance with Jupiter (hereafter the J3:1).

[Walsh et al. \(2013\)](#) also identified a possible second family, older and more dispersed, that was even closer to the  $\nu_6$  resonance than the Eulalia family. By identifying a plausible dynamical connection between many low albedo objects and (142) Polana, they dubbed this collection the "New Polana" family. Interestingly, this family not only includes some objects previously identified as part

of the old Polana family, but it also provides a plausible source for the vast majority of small dark background asteroids found at low inclinations near the  $\nu_6$  resonance. Here we consider both the Eulalia and New Polana families as a possible source for Bennu. According to estimates by [Walsh et al. \(2013\)](#), the Eulalia and New Polana families were 900–1500 Ma and over 2000 Ma, respectively. These values were based on several assumptions that will be revisited in the text below.

In addition to these older, spread out families, there are also several younger low albedo low inclination families that must also be considered as prospective sources for Bennu. The Erigone family is located in the inner main belt and is a few hundreds of Myr old, according to [Vokrouhlický et al. \(2006a\)](#). Like the families discussed above, its members have albedos and spectroscopic signatures that are not unlike those of Bennu ([Binzel, 2013](#), personal communication). In addition, the little-explored low inclination and albedo Clarissa and Sulamitis families, the latter which is roughly the same size and age as the Erigone family, must also be considered candidate sources for Bennu. Finally, it is possible that Bennu has no connection to a prominent asteroid family seen today, but instead was a denizen of the diffuse low albedo asteroid population currently seen in the inner main belt at modest to high inclinations.

While these new considerations are already enough to prompt a re-investigation of the source of Bennu, there are other motivations as well. No group has yet modeled the dynamical evolution of Bennu-sized bodies from the candidate families above to Bennu's current orbit. As we will show at some length below, this is a surprisingly challenging problem.

Consider that few constraints for the dynamical and spin vector evolution of  $D \approx 0.5$  km bodies are actually known. Sub-kilometer bodies remain largely below the observational detection limit of present-day telescopic surveys. We also do not know the thermal parameters that typical Bennu-sized bodies have in the main belt, and these parameters are needed to tell us how these bodies are affected by non-gravitational forces like the Yarkovsky and YORP effects (e.g., [Bottke et al., 2006a](#)). At present, the best we can do is infer their properties based on what we know of small asteroids in the NEO population. The biggest problem, however, is that our knowledge of how small asteroids evolve by the Yarkovsky and YORP effects are incomplete. As we will show below, existing models, as defined by [Vokrouhlický et al. \(2006a\)](#), cannot reproduce several distinctive features of older families. This motivated us to make the model modifications discussed in detail below.

Here we use our latest dynamical tools to quantitatively search for the source of Bennu. The organization of our paper is as follows:

**Section 2.** We discuss what is known about Bennu that can help us winnow down its possible main belt starting locations and family sources.

**Section 3.** We employ dynamical simulations to identify the source regions and orbital properties most likely to deliver a main belt asteroid to a Bennu-like orbit.

**Section 4.** We discuss the properties of the low albedo asteroid families in the inner main belt that are candidates to have produced Bennu: Clarissa, Erigone, Eulalia, New Polana, and Sulamitis.

**Section 5.** We discuss the dynamical evolution of bodies in our candidate families using two models. The first model contains the Yarkovsky and YORP effect descriptions provided by [Vokrouhlický et al. \(2006a\)](#). We call this the "static YORP" model because it assumes YORP torques do not change until the body reaches an endstate (i.e., spins up so fast it sheds mass; spins down so fast that collisions can reset its spin vector). The second is a modified model that implements the conclusions from [Statler \(2009\)](#). We call this the "stochastic YORP" model because it assumes YORP torques on an asteroid can be strongly modified by cratering events and shape changes caused by increases or decreases in the body's rotational angular momentum budget.

**Section 6.** We apply our stochastic YORP model to all of our candidate source families for Bennu, and estimate the ages of the most likely Bennu source families. We then calculate the fraction of Bennu-like asteroids from the families that are expected to contribute to two major escape routes: the  $\nu_6$  secular resonance, and the 7:2 and 5:9 overlapping mean motion resonances with Jupiter and Mars, respectively (hereafter J7:2/M5:9, with the first letter corresponding to the planet producing the resonance).

**Section 7.** We apply our results to other low albedo asteroids for sample return missions, namely (162173) 1999 JU3, linked to Hayabusa 2, and (175706) 1996 FG3, formerly the target of ESA's Marco Polo-R mission. We also discuss some of the implications of our stochastic YORP model for the shapes of small asteroids.

## 2. Bennu's physical parameters as constraints on its origin

Many of Bennu's evolutionary steps can be deduced from its existing physical properties using our current understanding of Solar System dynamics and collisional physics. Here we summarize Bennu's known constraints relevant for our work.

### 2.1. Orbit

The semimajor axis, eccentricity, and inclination of Bennu is  $(a, e, i) = (1.126 \text{ AU}, 0.204, 6.035^\circ)$ , respectively. Using the debiased NEO model of Bottke et al. (2002a), it is possible to gauge, in a probabilistic sense, its likely source region through which this asteroid has left the main belt.

The Bottke et al. (2002a) model assumes that NEOs with  $a < 7.4 \text{ AU}$  and absolute magnitude  $H < 22$  were derived from one of five primary source regions: the  $\nu_6$  secular resonance along the inner edge of the main belt, the intermediate source Mars-crossing region (IMC), the J3:1 mean motion resonance with Jupiter at 2.5 AU (J3:1), the outer main belt region (OB) beyond 2.8 AU, and the Jupiter Family Comet region (JFC), which is resupplied by the scattered disk in the transneptunian region. The dynamical pathways taken by numerous test bodies from these source regions were tracked across a network of cells in semimajor axis  $a$ , eccentricity  $e$ , and inclination  $i$  space (i.e., widths of  $0.05 \text{ AU} \times 0.02 \times 5^\circ$ ). The length of time spent by a particle in each cell was tabulated, yielding a “residence time” probability distribution for each source. These sources were then combined together with weighting functions and observational selection effects in order to compare them with NEO data. The best fit obtained by Bottke et al. (2002a) represents the current steady state orbital distribution of NEOs coming from that region, with peaks indicating where objects are statistically likely to be found in  $(a, e, i)$  space.

By comparing the  $(a, e, i)$  orbit of Bennu with this model, we found that it had a 82% and 18% probability of reaching its current orbit through the  $\nu_6$  resonance and IMC regions, respectively. Accordingly, the likely departure point of Bennu from the main belt was probably near 2.2 AU along the innermost edge of the main asteroid belt.

In addition, Campins et al. (2010) used the dynamical test body runs from Bottke et al. (2002a) to further investigate how inclination might further narrow the source of Bennu. They found that the test bodies best able to mimic the  $(a, e, i)$  parameters of Bennu came from starting orbits with low inclinations ( $< 10^\circ$ ). This rules out high inclination sources (e.g., Pallas family) as a plausible candidate to produce this NEO.

### 2.2. Size and spin vector

Radar and lightcurve observations tell us that Bennu has a mean diameter  $D \approx 0.5 \text{ km}$  (e.g., Nolan et al., 2013). This is small enough to be reasonably mobile via the Yarkovsky effect, but not so mobile

that it would easily be able to jump across major resonances (e.g., Bottke et al., 2000). This places the likely source of Bennu in the inner main belt between 2.1 and 2.5 AU.

The spin period of Bennu is fairly rapid ( $P = 4.3 \text{ h}$ ), while its shape is roundish with a equatorial waistband (Nolan et al., 2013). This consistent with the YORP spin up mechanism causing downslope movement, mass shedding, and possibly a satellite in the past (e.g., Walsh et al., 2008, 2012a; Vokrouhlický and Nesvorný, 2008; Pravec et al., 2010; Jacobson and Scheeres, 2011). If Bennu had a satellite until recently, it was most likely lost via Earth close encounters (Bottke and Melosh, 1996; Morbidelli et al., 2006).

The obliquity of Bennu is  $\delta \approx 180^\circ$  (Nolan et al., 2013), a common endstate value for objects that have been heavily influenced by YORP torques (e.g., Čapek and Vokrouhlický, 2004; Bottke et al., 2006a). Using Bennu's obliquity, we can infer a bit of its evolutionary history, at least in a statistical sense. Recall that the Yarkovsky effect causes the objects to migrate outward if their obliquity values are prograde or inward if they are retrograde. Interestingly, the majority of NEOs like Bennu have retrograde spins ( $\sim 70\%$ ; La Spina et al., 2004; see also Nugent et al., 2012 and Farnocchia et al., 2013). Using what we know of the Yarkovsky effect and main belt resonances, this value can be deduced using the Bottke et al. (2002a) model. The  $\nu_6$  resonance, which defines the innermost edge of the asteroid belt, provides about 37% of all NEOs with  $a < 7.4 \text{ AU}$ . The primary way for asteroids to reach it is by drifting inward, which mean they have to have a retrograde spin vector. All other NEO sources can be reached by inward and outward-drifting bodies; all things being equal, we would expect them to produce a 50–50 mix of prograde and retrograde NEOs. Putting these values together, we find the NEO population should be made up of  $\sim 70\%$  retrograde spins. Similarly, the probability factors above indicate a body on the same  $(a, e, i)$  orbit as Bennu has a 90% chance of having a retrograde spin axis. This matches observations, though Bennu is only a single data point.

### 2.3. Taxonomy, composition, and bulk density

The visible and infrared spectra of Bennu, defined as a B-type asteroid, indicates its bulk composition should be analogous to primitive carbonaceous chondrite meteorites, specifically CI and CM chondrites (Clark et al., 2011). This is consistent with Spitzer infrared observations of Bennu; thermal modeling of this data indicates it has an albedo of about  $4.3 \pm 0.3\%$  and a moderately low surface thermal inertia of  $310 \pm 70 \text{ J m}^{-2} \text{ s}^{-1/2} \text{ K}^{-1}$  (Emery et al., 2014). Detection of the orbital displacement produced by the Yarkovsky effect on Bennu has also led to an estimate of its bulk density, which is  $\rho = 1.26 \pm 0.21 \text{ g cm}^{-3}$  (Chesley et al., 2014). This value is consistent with many other C-complex asteroids (Britt et al., 2002).

Until very recently, Bennu's thermal inertia was thought to be  $600 \pm 70 \text{ J m}^{-2} \text{ s}^{-1/2} \text{ K}^{-1}$  (Emery et al., 2012; Mueller et al., 2012). This yielded a bulk density from Yarkovsky displacement of  $\rho = 1.0 \pm 0.15 \text{ g cm}^{-3}$ , assuming Bennu's mean rate of semimajor axis change  $|da/dt| = 2 \times 10^{-3} \text{ AU Myr}^{-1}$ . This value was used in our extensive simulations before the revised value was known. Fortunately, bulk density and thermal conductivity trade off of one another to produce similar Yarkovsky drift rates. This means our results are broadly consistent with a density  $\rho = 1.26 \pm 0.21 \text{ g cm}^{-3}$  value as well.

Put together, it would appear that Bennu came from a low albedo source whose fragments have access to main belt resonances in the innermost main belt region. Moreover, Bennu's small size, fast spin rate, top-like shape, and obliquity are all consistent with the idea that it has been significantly modified by YORP over time.

### 3. Using dynamics to better determine the source of Benu

The dynamical modeling work described by Bottke et al. (2002a) and used by Campins et al. (2010), predict the likely source region of Benu with reasonable accuracy. Nevertheless, certain aspects of their modeling work can be called into question. (We caution the reader that this section is fairly technical, such that those wishing to avoid the computational and modeling details can skip to the summary at the end).

First, Bottke et al. (2002a) assumed their test asteroids reached resonance via direct injection from an asteroid collisions, and thus they started most of their bodies deep within the J3:1 and  $\nu_6$  resonances. In reality, objects drift into those resonances via Yarkovsky thermal forces and may never reach the most chaotic regions. It is possible this assumption could affect their results. Second, Bottke et al. (2002a) assumed that fairly uniform distributions of test bodies were injected into the J3:1 and  $\nu_6$  resonances in terms of inclination. In reality, the input flux into these NEO sources depends on the asteroid population adjacent to those regions, with certain inclinations favored over others. Third, it is possible the runs in Bottke et al. (2002a) were too limited to resolve those starting inclinations favored to reproduce the  $(a, e, i)$  orbit of Benu (i.e., for their  $\nu_6$  resonance runs, Bottke et al. chose starting inclinations for their test bodies of  $i = 2.5^\circ, 5^\circ, 7.5^\circ, 10^\circ$  and  $12.5^\circ$ ). It would be useful to determine if other  $i$  values can succeed as well.

To determine whether these differences matter, we initiated several sets of runs from the three primary source regions defined by Bottke et al. (2002a): the  $\nu_6$  resonance, the J3:1 resonance, and the IMC region. Our starting population of test bodies for these regions was drawn from the numbered asteroids found in the Lowell observatory asteroid-orbit database (ASTORB; e.g., Bowell et al., 1994) with absolute magnitude  $H < 18$ . This value is fairly close to the detection limit for asteroid surveys.

For the  $\nu_6$  resonance, we selected from the above set bodies that resided within 0.05 AU of the anti-sunward side of the  $\nu_6$  boundary that were not on Mars-crossing orbits (assumed here to be perihelion  $q > 1.66$  AU) and that had  $i < 17^\circ$  (Fig. 1). For reference, the  $\nu_6$

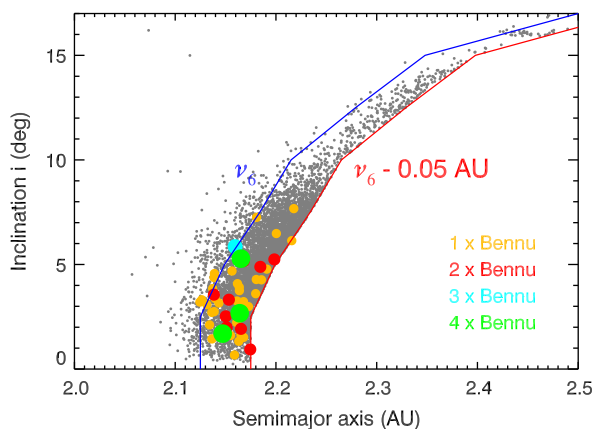


**Fig. 1.** The starting conditions of our model asteroids near the  $\nu_6$  resonance. The blue lines marks our definition of the  $\nu_6$  resonance (see Bottke et al., 2002a and the main text). The red line corresponds to orbits within 0.05 AU of the  $\nu_6$  resonance. The gray dots represent the known main belt asteroids with absolute magnitude  $H < 18$  found inside of the red line (6396 asteroids) with inclination  $i < 17^\circ$ . These objects were assigned sizes of  $D = 0.1$  and  $1$  km and were given the Yarkovsky drift rates  $da/dt = -2.5 \times 10^{-3}$  AU Myr $^{-1}$  and  $-2.5 \times 10^{-4}$  AU Myr $^{-1}$ , respectively. The colored circles represent the starting orbits of the model asteroids that reached within  $\Delta a \leq 0.01$  AU,  $\Delta e \leq 0.01$ , and  $\Delta i \leq 1^\circ$  of the semimajor axis  $a$ , eccentricity  $e$ , and inclination  $i$  of Benu's orbital parameters of  $(a, e, i) = (1.126$  AU,  $0.204$ ,  $6.035^\circ)$ . Their size and color correspond to the number of timesteps our model asteroids spent within our orbital match criteria. Note that most of the model asteroids have relatively low inclinations. (For interpretation of the references to color in this figure legend, the reader is referred to the web version of this article.)

boundary was defined by Bottke et al. (2002a) using numerical runs from Morbidelli and Gladman (1998); main belt test particles residing beyond the following  $(a, i)$  limits can reach planet-crossing orbits in less than  $\sim 1$  Myr:  $(2.125$  AU,  $0^\circ)$ ,  $(2.125$  AU,  $2.5^\circ)$ ,  $(2.149$  AU,  $5^\circ)$ ,  $(2.184$  AU,  $7.5^\circ)$ ,  $(2.215$  AU,  $10^\circ)$ ,  $(2.279$  AU,  $12.5^\circ)$ ,  $(2.348$  AU,  $15^\circ)$ , and  $(2.5$  AU,  $17.2^\circ)$ . This left us with 6396 asteroids. Note that an alternative method to define this resonance boundary can be found in Carruba (2010).

For the J3:1 resonance boundary, which makes something of a V-shape centered on 2.5 AU, we used the boundary conditions provided by Nesvorný (personal communication; see also Nesvorný et al., 2002a). Objects were drawn from the region within 0.05 AU of both far sides of the resonance. We also assumed they were not on Mars-crossing orbits, though we were more liberal with inclination ( $i < 27^\circ$ ). This left us 4092 asteroids. Note that we do not plot our starting conditions here, for reasons that will be explained below.

For the IMC region, which is a clearinghouse for small main belt resonances, we concentrated on asteroids in the inner main belt with orbital parameters with  $2.1 < a < 2.5$  AU,  $1.3 < q < 1.7$  AU, and  $i < 40^\circ$ . This gave us 7918 objects, with these bodies containing the Mars-crossers excluded from the other sets (Fig. 2). With that said, there is some unavoidable contamination here by objects from the  $\nu_6$  and J3:1 resonances, given the complicated nature of this space. Moreover, some IMC objects end up escaping onto NEO orbits ( $q < 1.3$  AU) via the  $\nu_6$  and J3:1 resonances. Despite these issues, Bottke et al. (2002a) argued that IMC region could largely be considered a distinct source region.

Using these test bodies, we employed the symplectic  $N$ -body code SWIFT-RMVS3 (e.g., Levison and Duncan, 1994), modified to accommodate Yarkovsky thermal forces (e.g., Vokrouhlický and Nesvorný, 2008), to track the evolution of test asteroids either entering into the  $\nu_6$  and J3:1 resonances or evolving within the IMC region. For now, we assumed these bodies were not affected by the YORP effect. In the code, the Yarkovsky drift rate for Benu-like objects is a preset variable whose value depends on many unknown parameters (e.g., spin vector, thermal conductivity, surface density, etc.). For these particular runs, rather than try to test all plausible Benu drift rate values, we instead decided to explore two sets of runs that bracket the plausible  $|da/dt|$  values:  $2.5 \times 10^{-3}$  AU Myr $^{-1}$  and  $2.5 \times 10^{-4}$  AU Myr $^{-1}$ . Note that the Benu's measured drift rate value,

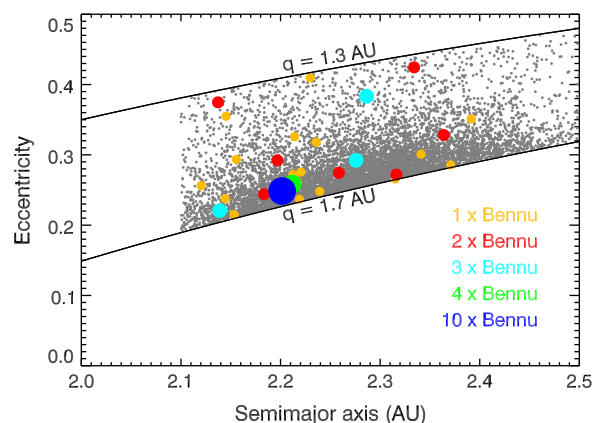


**Fig. 2.** The starting conditions of our model asteroids within the IMC region (see Bottke et al., 2002a). Here the region is defined as  $2.1 < a < 2.5$  AU, perihelion  $1.3 < q < 1.7$  AU, and  $i < 40^\circ$ . The gray dots correspond to 7918 known asteroids with  $H < 18$ . The model asteroids were assigned sizes of  $D = 0.1$  and  $1$  km. They were given Yarkovsky drift rates that bracket the plausible  $da/dt$  values:  $\pm 2.5 \times 10^{-3}$  AU Myr $^{-1}$  and  $\pm 2.5 \times 10^{-4}$  AU Myr $^{-1}$ , respectively. The colored dots are defined as in Fig. 1. (For interpretation of the references to color in this figure legend, the reader is referred to the web version of this article.)

$|da/dt| = 2 \times 10^{-3}$  AU Myr<sup>-1</sup>, scaled to a heliocentric distance of  $\sim 2.3$  AU, yields  $\sim 4 \times 10^{-4}$  AU Myr<sup>-1</sup>. The drift direction of the test asteroids were set so they would enter into the  $\nu_6$  or J3:1 resonance at these rates. For the IMC region, we gave the objects a random spin axis orientation that varied the preset  $|da/dt|$  value by  $\cos \delta$ .

For those test asteroids that reached inner Solar System, we checked to see which ones passed close to the current Benu's current  $(a, e, i)$  parameters (1.126 AU, 0.204, 6.035°) (see Figs. 1 and 2). A good match was arbitrarily defined as those with  $\Delta a \leq 0.01$  AU,  $\Delta e \leq 0.01$ , and  $\Delta i \leq 1^\circ$ . Combining all of our runs together, we found 65 test bodies ended up matching our criteria, nearly all from the  $\nu_6$  resonance (33 test asteroids) or IMC region (30 test asteroids). Some test bodies also matched Benu at more than a single timestep interval. This factor will be applied below when analyzing possible Benu starting orbits. Thus, if a test asteroid from a given starting  $(a, e, i)$  matches Benu six times over the course of its lifetime, we also weight its contribution by a factor of six. Only two particles came from the J3:1 resonance, consistent with the Bottke et al. (2002a) results suggesting this was an unlikely source for Benu.

Our results also indicate that our different choices for our test asteroid drift rates did not significantly affect the number of objects reaching Benu-like orbits from any source region. In the results discussed below, we combine our different drift rates runs together when discussing each source. We also interpret the test body matches for the  $\nu_6$  and IMC regions separately, partly because the runs started with different numbers of test bodies but also because the source probability model of Bottke et al. (2002a) strongly favored the  $\nu_6$  resonance as a source of Benu (82–18%). To evaluate the two sources defined above against one another, we would have to weight them within a Bottke et al. (2002a)-like model that (i) accounted for observations biases and (ii) fit our results to the observed NEO population.

For the  $\nu_6$  resonance, we find that 100% of our Benu matches came from main belt test asteroids that had starting  $i < 8^\circ$  (Fig. 1). Most of the matches (90%) were found between  $1^\circ < i < 6^\circ$ , with the distribution slightly favoring values between  $3^\circ$  and  $4^\circ$ . Moreover, about 95% of these matches had starting eccentricity  $e < 0.2$ , with clear preferences for values between 0.1 and 0.2, and semimajor axes  $a < 2.2$  AU. For the IMC region, we find values for starting  $i$  that match for  $< 11^\circ$ , though 77% of the probability has  $i < 7^\circ$  (Fig. 2). Here the starting  $e$  values are all  $> 0.2$  as part of the definition of the IMC region, while the starting  $a$  values are all  $< 2.4$  AU, with the majority (54%) between 2.2 and 2.3 AU.

These results, when considered with previous work by Walsh et al. (2013), allow us to say a number of things about the likely source of Benu. Walsh et al. (2013) argued that most small dark asteroids in the inner main belt with low inclinations are associated with known asteroid families. If true, Benu mostly likely came from an existing low albedo asteroid family residing in the inner main belt between 2.1 and 2.5 AU. This also implies that the background population of small low albedo asteroids in this region is probably negligible. Some characteristics of the Benu source family can therefore be deduced from our runs. We find the following.

- (1) The Benu source family should be a substantial source of asteroids whose albedo and spectroscopic signatures mimic the properties of Benu itself.
- (2) The family must be able to provide Benu-sized family members to the  $\nu_6$  resonance or the IMC region today. This implies that small families members have spread far enough

across the inner main belt by Yarkovsky thermal forces that Benu-sized objects ( $D \approx 0.5$  km) are now in contact with those source regions.

- (3) The family members should reside on osculating orbits ( $i < 7^\circ$ ) in the inner main belt between 2.1 and 2.5 AU, as suggested by previous work (Campins et al., 2010).
- (4) Of the three primary sources investigated here, strong preference should probably be given to the runs from the  $\nu_6$  resonance, according to the Bottke et al. (2002a) source predictor model. In those runs, the  $\nu_6$  resonance is favored as a source of Benu over that of the IMC region 82–18%.
- (5) The most likely source family will have osculating eccentricities between  $0.1 < e < 0.2$  and inclinations between  $1^\circ < i < 6^\circ$ , with a preference for  $3^\circ < i < 4^\circ$ .

In the next section, we will discuss the low albedo inner main belt families that provide the best fit to these preferences.

#### 4. Low albedo families in the inner main belt

The hierarchical clustering method (HCM; e.g., Zappalà et al., 1990, 1994; Knežević et al., 2002) has been used to identify asteroid families as clusters of objects in proper semimajor  $a$ , eccentricity  $e$ , and inclination  $i$  space. When HCM is applied to state of the art proper element databases, it is possible to identify more than 50 families of all sizes across the main belt region (e.g., Nesvorný, 2012; Brož et al., 2013; Masiero et al., 2013). The family members and background objects can also be paired with the trove of asteroid albedo data derived from WISE spacecraft observations (Masiero et al., 2011, 2013) and extensive photometric and spectroscopic datasets (e.g., Ivezić et al., 2002; Mothé-Diniz et al., 2005; Parker et al., 2008). Taken together, it is possible to sift the inner asteroid belt for candidate asteroid families that look similar to Benu and provide the best match to our dynamical criteria (1)–(4) above. Note that similar work was recently performed by Campins et al. (2013) when searching for the source of asteroid (162173) 1999 JU3.

To date, we have identified five prominent families consistent with our constraints: Erigone, Sulamitis, Clarissa, Eulalia, and New Polana. The proper  $(a, e, i)$  of these families are shown in Fig. 3. Here we briefly describe them.

##### 4.1. Erigone

The Erigone family is centered on the asteroid (163) Erigone (proper  $a = 2.367$  AU) and is located in the central region of the inner main belt. Fig. 4 shows 2513 family members that have been identified to date by HCM in  $(a, H)$ . The albedo distribution of Erigone members observed by WISE shows a peak in log space near  $\log p_v = -1.25$ , or at about 5.5% (Masiero et al., 2011), with numerous members matching the Benu albedo of  $4.3 \pm 0.3\%$ . According to the SPH/N-body modeling results of Durda et al. (2007) and Benavidez et al. (2012), the mean parent body size of Erigone was 90–110 km diameter, large enough that it could supply numerous Benu-sized bodies to the inner Solar System if family members have reached one of the NEO source regions described above.

As described in detail by Vokrouhlický et al. (2006a), the family shows abundant signs that it has experienced dynamical spreading via the Yarkovsky thermal forces, with their  $da/dt$  drift rates affected by YORP spin vector evolution. The family is divided into two fragment clouds, or what we colloquially call “ears”, separated by a depletion in the center.

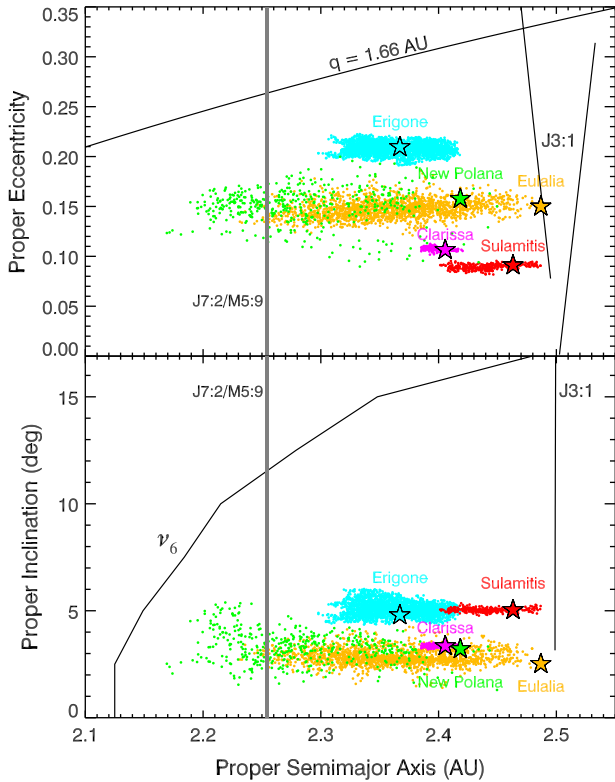


**Fig. 3.** The low albedo asteroid families in the inner main belt that could have plausibly produced Benu. The top figure shows their proper  $a$  and  $e$  values, while the bottom figure shows proper  $i$ . The asteroid families, Clarissa, Erigone, Eulalia, New Polana, and Sulamitis, were defined using data and analysis from Nesvorný (2012), Masiero et al. (2011) and Walsh et al. (2013). The filled stars are inferred central bodies of each family: (302) Clarissa, (163) Erigone, (495) Eulalia, (163) Polana, and (752) Sulamitis. The approximate boundaries of the  $\nu_6$  secular resonance and J3:1 mean motion resonance with Jupiter are shown as solid lines. We also show one of the most powerful resonances capable of feeding the IMC region, the overlapping 7:2 and 5:9 mean motion resonances with Jupiter and Mars, respectively (J7:2/M5:9) Nesvorný and Morbidelli (1998). The  $q = 1.66$  AU line is the orbit needed to cross the orbit of Mars with its current osculated eccentricity.

To create these features, we assume that immediately after Erigone disrupted, the debris began to spread out in semimajor axis by the Yarkovsky effect, with smaller bodies drifting inward toward or outward away from the Sun faster than larger bodies (Bottke et al., 2006a; Vokrouhlický and Bottke, 2012). At the same time, the YORP effect preferentially tilts their obliquities toward  $0^\circ$  or  $180^\circ$ , values that optimize their  $da/dt$  drift rates. This allows the Yarkovsky–YORP effects over time to mold the family into a two-lobed structure in  $(a, H)$ , with each lobe filled with fast-moving asteroids headed away from the family center.

Using a Monte Carlo code that characterizes Yarkovsky–YORP evolution, Vokrouhlický et al. (2006a) was able to reproduce these family features and estimate the Erigone family’s age. We will review this issue later in the paper. The question is whether Benu-sized bodies have drifted far enough from Erigone to reach either  $\nu_6$  resonance or the IMC source regions. As shown by Fig. 4, answering this is problematic because we have almost no family data for  $H > 19$ . Our method to address this issue is discussed in the next section.

#### 4.2. Sulamitis and Clarissa

The Sulamitis family appears to be roughly comparable in semimajor axis breadth to the Erigone family (Fig. 5). The brightest member, (752) Sulamitis, is located at proper  $a = 2.463$  AU near

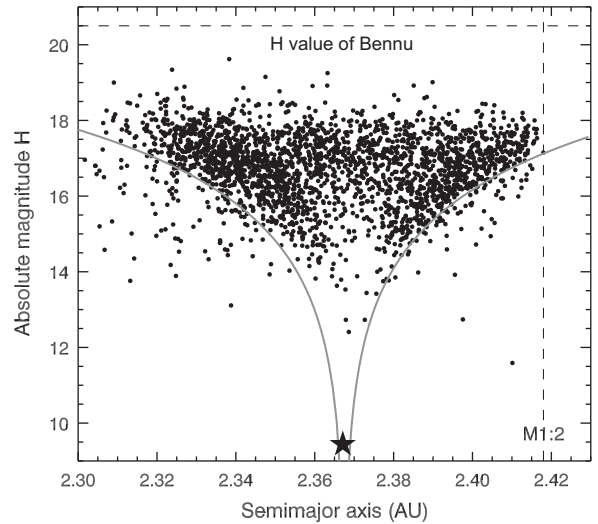


**Fig. 4.** The Erigone family. The 2513 family members are shown in semimajor axis  $a$ , absolute magnitude  $H$  space  $(a, H)$ . The star represents the inferred largest remnant and central body (163) Erigone. The solid lines were calculated using Eq. (1), and they correspond to  $C = 1.9 \times 10^{-5}$  AU. They roughly bracket the fastest members of the family using Yarkovsky–YORP theory. These effects have separated the family into two clouds with  $a < 2.37$  AU and  $a > 2.37$  AU. Two prominent clusters of bodies, or ears, are found near the gray lines. They are the expected byproduct of a family evolving by the Yarkovsky and YORP effects (e.g., Vokrouhlický et al., 2006a). The  $H$  value of Benu and the location of the Mars 1:2 mean motion resonance are also shown as dashed lines. Objects below the V-shaped lines are likely family interlopers.

the outer edge of the inner main belt. The family has not been well studied, and only has 294 known members.

While Durda et al. (2007) provide no information on its likely parent body size, the paucity of Sulamitis members compared to Erigone imply the family is smaller than Erigone, though their slightly larger heliocentric distances and lower orbital eccentricities may make them more difficult to be discovered. Brož et al.

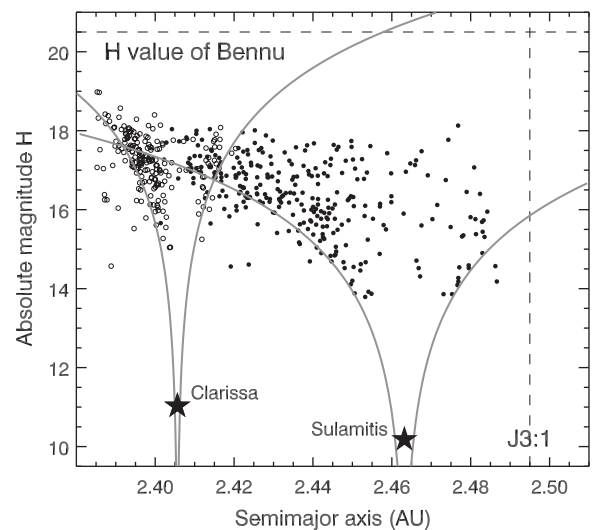


**Fig. 5.** The Clarissa and Sulamitis families. Only 202 and 294 members of the family have been identified to date, respectively. The stars are (302) Clarissa and (752) Sulamitis. The solid lines were calculated using Eq. (1), and they correspond to  $C = 4.15 \times 10^{-6}$  AU and  $2.15 \times 10^{-5}$  AU, respectively. They roughly bracket the fastest members of the family using Yarkovsky–YORP theory. The  $H$  value of Benu and the location of the J3:1 mean motion resonance with Jupiter are shown as dashed lines. This plots suggests that many Sulamitis family members have been lost by drifting into the J3:1 resonance by the Yarkovsky effect.

(2013) estimated the parent body was  $D \sim 65$  km, indeed some 15–25% smaller than the diameter of the Erigone family's parent body. As with Erigone, the albedo distribution of members observed by WISE peaks in log space near  $\log p_v = -1.25$ , or at about 5.5% (e.g., Masiero et al., 2011).

The family is asymmetric, with the right side partially truncated by the J3:1 resonance (Fig. 5). We deduce that family members moving outward away from the Sun were lost as the Yarkovsky effect drove them into the J3:1. The age of the family is unknown, but the Yarkovsky V-shaped curve drawn to adhere to the left ear of the family (i.e., with semimajor axis less than that of the largest remnant of the family) indicates it is about as old as Erigone.

The Clarissa family, connected with (302) Clarissa at  $a = 2.406$  AU, appears to be younger, smaller, and more compact compared to Erigone and Sulamitis. It has 202 known members. Clarissa is included in this study for completeness, but it can probably be ruled out as a candidate to produce Bennu by inspection alone, unless some objects can escape via the nearby 1:2 mean motion resonance with Mars.

#### 4.3. Eulalia, or the “Original Polana” family

The Eulalia family (Fig. 6), often referred to as the Polana family in the literature, represents the primitive component of the Nysa–Polana complex (Cellino et al., 2001, 2002; Campins et al., 2010, 2013; Gayon-Markt et al., 2012; Walsh et al., 2013). As shown in Figs. 3 and 6, the largest remnant in the Eulalia family is now thought to be (495) Eulalia, which is located on the brink of the J3:1 resonance with  $a = 2.487$  AU.

Prior to Walsh et al. (2013), (495) Eulalia had not previously been associated with the low albedo part of the complex. This is because (495) Eulalia's eccentricity had diffused over hundreds of millions of years via a combination of the Yarkovsky effect and narrow resonances located near the J3:1 (see Walsh et al., 2013). Its membership in the family was determined in a probabilistic fashion. Another complication in understanding the Eulalia family is that the right half of it is missing; many family members evolving

outward from the Sun by the Yarkovsky effect were ejected from the main belt via the J3:1.

A full description of the characteristics of the Eulalia family can be found in Walsh et al. (2013). Summarizing their results, they find that Eulalia members have albedos similar to those of Erigone and Sulamitis (Masiero et al., 2011, 2013; Walsh et al., 2013). The parent body size, estimated using the techniques of Durda et al. (2007), was approximately  $D \sim 100$ –160 km. The age of the family was estimated to be 900–1500 Myr old using estimates that took advantage of the Yarkovsky V-shaped curves shown in Fig. 6.

#### 4.4. New Polana

WISE observations suggest that there is a substantial background population of low albedo asteroids with access to the  $\nu_6$  resonance and IMC region of the main belt (Masiero et al., 2011). Many of these bodies are located at  $i > 7^\circ$ , making them poor candidates to deliver Bennu to its observed orbit (see summary of results from the last section). Those at  $i < 7^\circ$ , however, cannot be ruled out so quickly, and they could conceivably dominate the contribution of Bennu-like objects. Intriguingly, their characteristics, as defined by Walsh et al. (2013), are not random. Using dynamical arguments, it is reasonable to suggest many are family members associated with (142) Polana (Fig. 7).

Consider that in Fig. 3, we find an apparent paucity of low albedo asteroids with  $a < 2.3$  AU and  $H < 14$ . At the same time, we also see a surprisingly high density of objects with  $15 < H < 17$  and  $2.1 < a < 2.3$  AU. The location of these bodies in  $(a, H)$  makes them appear to be the left ear of an asteroid family whose largest remnant is (142) Polana. Thus, Polana may indeed have a family, just not the one that was expected.

Several factors allowed the putative New Polana family to be missed by observers and dynamicists over the years. First, the family appear to be old and dispersed; Walsh et al. (2013) estimates its age to be  $\sim 2$  Gyr old. This leaves ample time for the smaller family members to evolve across the forest of resonances located in the inner main belt. These interactions probably caused their  $e$  and  $i$  values to move away from their starting values. This would explain

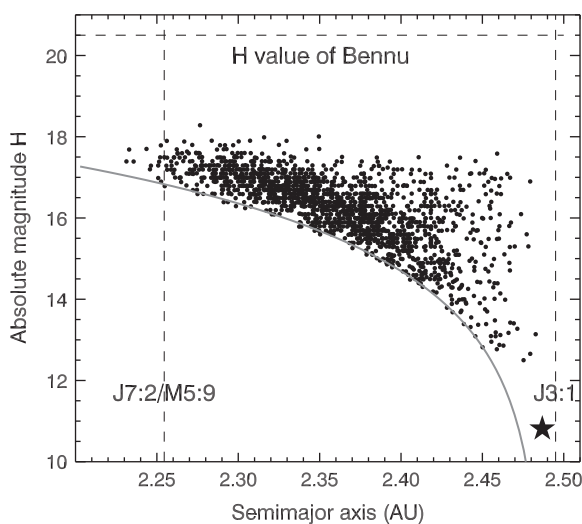


**Fig. 6.** The Eulalia family. This family was defined by Walsh et al. (2013), and the dots show 1676 family members. The star represents (495) Eulalia, which is located on the brink of the J3:1 resonance with  $a = 2.487$  AU. The solid lines were calculated using Eq. (1), and they correspond to  $C = 10^{-4}$  AU. The  $H$  value of Bennu and the location of the J3:1 mean motion resonance with Jupiter are shown as dashed lines. Walsh et al. (2013) argue that we are only looking at the left ear of the family, with the right ear eliminated by the J3:1 resonance by direct injection and by objects drifting into the resonance by the Yarkovsky effect.

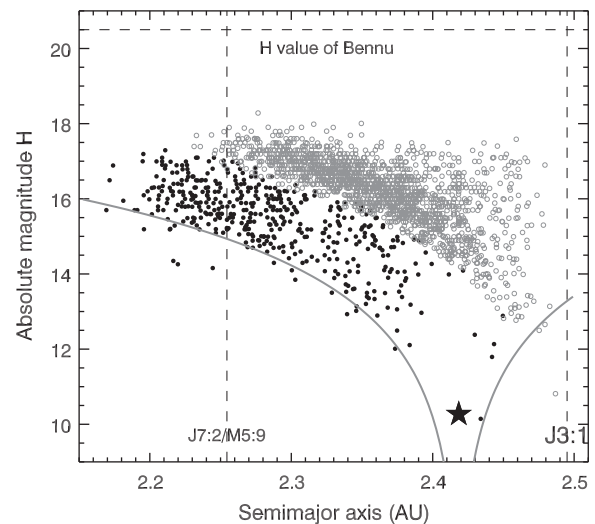


**Fig. 7.** The New Polana family. This family was defined by Walsh et al. (2013), with the black dots showing 444 family members. For reference, the open circles show the Eulalia family (Fig. 6). The star represents (142) Polana. The solid lines were calculated using Eq. (1), and they correspond to  $C = 1.69 \times 10^{-4}$  AU. The  $H$  value of Bennu and the location of the J3:1 mean motion resonance with Jupiter are shown as dashed lines. As with the Eulalia family, Walsh et al. (2013) argue we are mainly seeing the remnants of the left ear of the family. Most of the right ear was lost when outward-drifting objects entered the J3:1 resonance by the Yarkovsky effect.

why New Polana objects in Fig. 3 are quite diffuse compared to the other families. Second, the family has nearly the same eccentricity, inclination, color, and albedo distribution as the Eulalia family. This means cross-contamination between the families is unavoidable; some of the Eulalia family members shown as gray open circles in Fig. 7 must in reality be New Polana family members. Sorting out the families is extremely difficult, especially when we lack a detailed spectral analysis of all candidate objects. Third, nearly all of the analysis in Walsh et al. (2013) could not have been accomplished without the WISE-derived albedo data (e.g., Masiero et al., 2011). We have only scratched the surface of what can be done with this remarkable data set.

The size of the New Polana parent body has not yet been calculated. This complicates efforts to determine the source of Bennu. As we will discuss below, however, sufficient data exists to at least deal with this issue in an approximate manner.

## 5. Modeling the evolution of low albedo asteroid families

To identify the source of Bennu from the low albedo families described above, we need to estimate the flux of Bennu-sized asteroids from each family to the  $\nu_6$  resonance and IMC regions over time. This is easier said than done, particularly when you consider that Bennu is much dimmer than the low albedo family members observed in the inner main belt. This leaves us with few direct constraints on the Yarkovsky drift rates of typical Bennu-sized bodies (e.g., Nugent et al., 2012; Farnocchia et al., 2013) and even less information on how they evolve in reaction to YORP (e.g., Vokrouhlický and Bottke, 2012).

Just as important, we only have a limited understanding of what happens to asteroids of all sizes that spin up so fast that they shed mass or spin down so slowly that they enter into a tumbling rotation state. The critical question for Bennu's evolution, and that of other small asteroids, is how to treat their evolution through these YORP endstates, or what we hereafter call "YORP cycles" (e.g., Rubincam, 2000).

Our goal in this section is to create a reasonable Yarkovsky/YORP asteroid family evolution model that reproduces the important observed characteristics of the low albedo families in Fig. 3. Once accomplished, we can plausibly argue that our model results can be extrapolated down to smaller, Bennu-size bodies, where constraints are limited.

As an aside, the model presented here concentrates on the dominant effects capable of modifying the semimajor axes of multikilometer- and smaller asteroids. For this reason, we do not include here the effects of encounters with massive asteroids (e.g., Carruba et al., 2003, 2013 and similar reference therein) and collisions capable of modifying the orbits of asteroids (e.g., Dell'Oro and Cellino, 2007). The passage of migrating asteroids through weak mean motion and secular resonances in the inner main belt, which may modestly affect their eccentricities and inclinations (e.g., Bottke et al., 2001; Carruba et al., 2005), were also neglected, partly because including them is computationally expensive but also because most do not strongly affect the delivery rate of small asteroids to powerful resonances capable of delivering them to planet-crossing orbits.

As a starting point, we turn to the work done by Vokrouhlický et al. (2006a,b,c) (see also Bottke et al., 2007). They have used Monte Carlo codes to track how Yarkovsky–YORP forces/torques affect the dynamical evolution of model asteroids. In the process, they have calculated the ages of young families that are only a few hundreds of Myr old. Specifically, they allowed  $D \approx 3 - 10$  km family members to evolve in semimajor axis until their distribution in  $(a, H)$  space adequately matched the observed family.

The advantage of this code is speed; it allows us to track tens of millions of asteroids over reasonable computation timescales. The downside is that it does not track the effects of planetary resonances on our model asteroids'  $e$  and  $i$  values. For the problems attacked in this paper, we consider this an acceptable trade off. Numerical tests show most  $e$  and  $i$  changes do not strongly affect a family's  $(a, H)$  constraints, unless the asteroid is pushed out of the family or out of the main belt altogether.

There are two components that determine a family's  $(a, H)$  distribution: (i) its initial ejection velocity field, and (ii) its post-formation dynamical evolution. For a given model asteroid, the Yarkovsky effect makes the semimajor axis increase or decrease with different speeds, depending on a number of parameters that includes the rotation rate and the obliquity. These latter are, in turn, affected by the strength of the YORP effect, which makes asteroid rotation rates increase or decrease and, at the same time tilts the obliquity towards the extreme values of  $0^\circ$  or  $180^\circ$ . The obliquity extremes maximize the Yarkovsky drift rates for the asteroids and "polarizes" them in  $(a, H)$  space, with smaller members preferentially populating extreme  $a$  values (i.e., the ears of the family). When an  $(a, H)$  configuration has been achieved that matches observations for a particular family, we can constrain the family's age and other initial parameters. Several worked examples of this procedure can be found in Vokrouhlický et al. (2006a,b,c).

As an aside, we point out that other endstate obliquities of YORP evolution are possible (e.g., including  $90^\circ$ ; see Vokrouhlický and Čapek, 2002; Scheeres and Mirrahimi, 2008). Simulations by Čapek and Vokrouhlický (2004), however, indicate that common thermal conductivity values for small asteroids produce a strong preference for extreme obliquity values.

### 5.1. Description of Yarkovsky–YORP Monte Carlo evolution code

The fine details of our Monte Carlo code can be found in Vokrouhlický et al. (2006a). Here we only describe enough model highlights that the reader can understand its basic operation.

First, we find it useful to redefine families in a parameter space that is well suited to make comparisons between model asteroids evolving by Yarkovsky–YORP forces and the known family members. Specifically, following Vokrouhlický et al. (2006a), we transform the 2-D  $(a, H)$  coordinates for a given family into a 1-D parameter called  $C$ , defined as:

$$0.2H = \log(\Delta a/C). \quad (1)$$

Here  $\Delta a = a - a_c$ , with  $a_c$  defined as the center of the family. In practice,  $a_c$  is often close to, or the same as, the semimajor axis value of the largest remnant of the family. However, because the latter might have also changed its semimajor axis position by the Yarkovsky effect, and also to obtain slightly less noisy data, we average the family's  $C$  distribution by taking  $a_c$  in a small interval around the central object (for instance, in the Eulalia-family case, we sampled an interval of 0.0015 AU near the nominal proper  $a$  value of 495 Eulalia). When  $C$  is equal to a constant, the curves obtained form a V-shape pattern in the  $(a, H)$  plane centered on the  $a_c$  value (Fig. 8).

The location of asteroids in the family can then be represented by a distribution function  $N(C)$ , such that there are  $dN = N(C)dC$  bodies in a given bin with boundaries of  $(C, C + dC)$ . The goal of our Monte Carlo model is to reconstruct and numerically match the  $N(C)$  function using a  $\chi^2$  method. In this fashion, the effects of varying our parameters can be better quantified.

As an aside, we note that there are other ways to compute the family's center (Carruba, 2013). Alternative methods may be needed when the position of the largest remnant is different from that inferred from the orbital distribution of the family members.

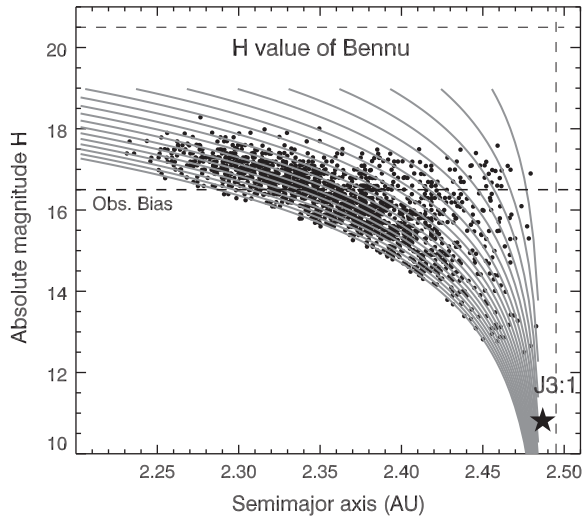


**Fig. 8.** The Eulalia family plotted with isoline curves where  $C = \text{const}$ . The lines define bins that will be used to characterize the family in  $N(C)$  (see text), with widths of  $5 \times 10^{-6}$  AU. The dashed line at  $H = 16.5$  corresponds to the region where observational selection effects may be influencing the family (i.e., objects with  $H > 16.5$  may be faint enough that the observed objects do not characterize the orbital distribution of the family). We do not use  $H > 16.5$  objects in our analysis of  $N(C)$ .

Reasons that the largest remnant would be displaced from the family center include peculiarities in the nature of the disruption event (e.g., Durda et al., 2004) and/or the dynamical evolution of the largest remnant via the Yarkovsky effect (e.g., Warner et al., 2009) or asteroid close encounters (e.g., Carruba et al., 2003).

Vokrouhlický et al. (2006a) defined several key parameters that control how model asteroids in the Monte Carlo code evolve over time. The first is the ejection velocity  $V$ , which they defined as  $V_{SD} = V(5 \text{ km}/D)$ , where  $V_{SD}$  is the standard deviation of a Gaussian velocity distribution for the family's fragments. They assume that  $V_{SD}$  is inversely proportional to size  $D$  (e.g., Nesvorný et al., 2002b; Nesvorný and Bottke, 2004; Michel et al., 2004; Durda et al., 2004).

The second parameter is  $c_{YORP}$ , which defines the strength of the YORP effect. By varying  $c_{YORP}$ , one can control how fast the asteroid's spin rate accelerates or decelerates and how fast its obliquity moves toward  $0^\circ$  or  $180^\circ$ . The reference strength of the YORP torques, to which the  $c_{YORP}$  parameter is applied, is given by functions that were originally derived from the work of Čapek and Vokrouhlický (2004) (see also the Appendix A).

The third parameter is the age of the family  $T$ , which controls how far the family members have drifted via Yarkovsky thermal forces since formation. Finally, there is the parameter  $\tau_{reorient}$ , the timescale for complete reorientation of the asteroid's spin vector via collisions. It is assumed in the code that non-catastrophic impacts can occasionally impart sufficient rotational angular momentum to an asteroid that its spin vector can be completely reset (see Farinella et al., 1998). Such events are much more likely to take place on slow-spinning asteroids than fast-spinning ones.

A critical unknown in our existing Yarkovsky–YORP formalism, which strongly affects older, more spread-out families, concerns what happens when our model asteroids reach their rotational endstates, namely when the rotation periods become very large or very small. For very slow spinning bodies, principal axis rotation breaks down, with the body entering into a tumbling rotation state (e.g., Vokrouhlický et al., 2007; Breiter et al., 2010). At the other extreme, fast spinning bodies with rotation periods approaching  $P \approx 2 - 3$  h may change shape, shed mass or undergo fission in an attempt to accommodate or lose rotational angular momentum.

Evidence for this latter behavior comes from observations of near-Earth and main belt binary asteroids, many whose primary is spinning remarkably close to the fission limit (e.g., Walsh and Richardson, 2006; Pravec and Harris, 2007), and the analysis of pairs of asteroids on extremely-similar heliocentric orbits (e.g., Vokrouhlický and Nesvorný, 2008). Pravec et al. (2010) showed that most asteroid pairs (if not all) had to form by rotational fission.

YORP cycles refer to the process of an asteroid entering into and eventually exiting a rotational endstate with a new spin vector. The duration of a YORP cycle, as well as its timescale to evolve from a given rotation state to a YORP endstate, is a quantity that requires more study. We assume it is a few times the YORP doubling timescale, which was defined by Rubincam (2000) to be the timescale needed for YORP to reduce an asteroid's spin rate in half. Obviously, both quantities are strong functions of the asteroid's size (approximately proportional to  $D^2$ ) and orbit.

Understanding YORP cycles is one of the most challenging aspects of modeling the evolution of both individual asteroids and asteroid families. If an object undergoes YORP cycles too frequently, the varying direction of the new spin axis will cause the body to experience a random walk in semimajor axis by the Yarkovsky effect. As we will show below, this effect can have serious implications for how asteroid families spread in semimajor axis over time.

To deal with YORP cycles in our code, we adopt the following necessarily simplified approach. As the rotation rate slows down via YORP, the rotation period  $P$  of our model asteroid eventually reaches a predefined critical limit  $P_{crit,1}$ . Here  $P_{crit,1} = 1000$  h. Once achieved, we freeze  $P$  at that value. In reality, the asteroid would enter into a non-principal axis rotation state, though we do not model this effect. Instead, we take advantage of the fact that the Yarkovsky effect becomes highly inefficient for such slowly-rotating bodies (e.g., Vokrouhlický, 1998, 1999). This means that we can treat this rotation state evolution phase using approximate methods without seriously impacting the delivery rate of asteroids into main belt escape hatches.

We assume an asteroid caught in this slow rotation phase escapes by undergoing a sub-catastrophic collision capable of redefining its rotational angular momentum vector. We test for the occurrence of such a reorientation event at every integration time-step once the body has reached  $P_{crit,1}$ . The characteristic timescale for this rotational reset event is defined as  $\tau_{reorient} = K P^{-5/6} D^{4/3}$ , with  $K$  a constant (Farinella et al., 1998). A nominal value of  $K = K_{nom}$  can be found in Eq. (11) of Vokrouhlický et al. (2006a), but since this value is only modestly constrained, we also use an empiric multiplication factor  $c_{reorient}$  of the order of unity, leaving  $K = c_{reorient} K_{nom}$  for our simulations. When a rotational reset event takes place, we reinitialize the spin vector of the asteroid, with the obliquity chosen randomly and  $P$  selected from a Maxwellian distribution with a characteristic (peak) value of 8 h. This is an expected outcome of this random process.

For  $P$  values that become very small, such that mass shedding is imminent on a rubble-pile asteroid, we define a second critical value  $P_{crit,2} \approx 2$  h where we assume the asteroid loses material and rotational angular momentum. In reality,  $P_{crit,2}$  should be a range of values between 2 and 4 h, depending on the elongated shape of the asteroid, but we neglect this effect here. We also do not simulate the production of a binary made up of two, nearly equal-size bodies, but instead assume the amount of mass shed from the primary is small enough to make no meaningful change to the size of the primary. This is arguably reasonable, given that most asteroid pairs have primary/secondary size ratios  $>5$ , therefore volume ratios of at least 100 (e.g., Pravec et al., 2010).

Taking the observed distribution of the mass-ratio  $q$  in asteroid pairs (e.g., Vokrouhlický and Nesvorný, 2008), we randomly select

a specific  $q$  value and then employ the rotation rate relationship  $\omega_{\text{final}}^2 = \omega_{\text{initial}}^2 - Kq$  to obtain a new rotation period for the asteroid (with  $K$  again a constant; simple theoretical justification of this formula and the approximate value of  $K$  can be found in the Supplementary Materials to Pravec et al., 2010). The slower rotation rate that the primary gets after a mass shedding event,  $\omega_{\text{final}} < \omega_{\text{initial}}$ , is due to angular momentum being carried away from the system by the ejecta. We also assume the mass shedding events are gentle enough that the obliquity of the parent body remains unchanged.

Finally, during collisional reorientation and mass shedding events, we assume the shape of the model asteroid has changed enough that a new shape function should be chosen from the available inventory of possibilities, as discussed in detail in Vokrouhlický et al. (2006a) (see also Appendix A). This means the body's YORP-induced spin rate and obliquity variations may take place more quickly or slowly than before the event.

All of this leads to the evolutionary tracks for the spin and shape that can become quite convoluted. For example, a given model asteroid might (i) spin up fast enough to shed mass, (ii) obtain a new rotation rate and shape after mass loss, and (iii) start to decelerate to a slower rotation rate via YORP torques that react to the asteroid's new shape, (iv) spin down enough to enter into a tumbling rotation state, and (v) undergo a collisional reorientation event, which allows the body to start again with a new shape and spin state. Thus, dramatic changes to the spin vector and drift direction of the asteroid may occur at both points (ii) and (v).

A key question is whether important events happen in-between the YORP endstates. In Vokrouhlický et al. (2006a,b), it was assumed that in this interval, the spin vector undergoes slow steady changes via YORP torques in one direction; always spinning up or always spinning down, with the spin axis orientation moving secularly toward  $0^\circ$  or  $180^\circ$ . Only the most dramatic collisions have an effect on the body's spin state. We call this approximation the "static YORP" model. The question of whether the static YORP model is valid will be addressed below.

## 5.2. Constraining the Static YORP Monte Carlo model

Our next task is to calibrate our static YORP model against the available spin period and obliquity constraints that exist for small asteroids. Our initial tests were designed to reproduce the rotation rate and pole orientation distributions of small main belt asteroids and NEOs. This means examining the effects of the parameters  $\tau_{\text{coll}}$  and  $c_{\text{YORP}}$  on our results. Our motivation for exploring  $c_{\text{YORP}}$  comes from the work of Rozitis and Green (2012), who have published a detailed numerical analysis of the YORP effect. They find that the effects of mutual irradiation of small-scale structures on the surface, such as crater-walls or nearby boulders, have a systematic tendency to decrease the YORP strength by as much as a factor of 2–3. These effects were not accounted for by Čapek and Vokrouhlický (2004).

Through model trial and error, as well as theoretical considerations, we have also identified an additional parameter needed to compare model results to data. We call it  $\delta_{\text{YORP}}$ , and it controls the asymmetry in the asymptotic acceleration or deceleration of the YORP effect (i.e., the fraction of small asteroids that are spinning up vs. spinning down).

Why is  $\delta_{\text{YORP}}$  needed? After all, Čapek and Vokrouhlický (2004) concluded that for bodies of sufficient surface thermal inertia, YORP was equally likely to produce asymptotic acceleration or deceleration of the rotation rate (i.e., a 50–50 mix). The reason is that this apparent balance may not be exact. Results by Golubov and Krugly (2010), who considered the putative effects of a transverse heat conduction through surface boulders and other

small-scale topography features, show that they may lead to a preference for asymptotic acceleration of the rotation rate.

On the other hand, Čapek and Vokrouhlický (2004) showed that low-enough thermal inertia values can lead objects to preferentially decelerate their rotation. It is unclear which of these effects should dominate among small asteroids with a wide variety of shapes. Therefore, by introducing  $\delta_{\text{YORP}}$ , we can test our static YORP model against data. (As an aside, we note that all five of the available direct detections of the YORP effect indicate rotation rate acceleration. We are concerned about a bias, though, that might prevent observers from obtaining YORP for slowly-rotating asteroids because their lightcurves are harder to measure).

For our runs, we generated 100 synthetic inner main belt asteroids (see Čapek and Vokrouhlický, 2004). We set their sizes to  $D = 1$  km. Their initial rotation poles were assumed to be random in space, while their rotation frequencies were selected from a Maxwellian distribution with a maximum corresponding to  $P = 8$  h. Note that these runs were insensitive to these initial conditions because YORP evolution quickly removes any memory of them. Their orbit and rotation vectors were tracked using our Monte Carlo code for 4000 Myr. We tested values of  $\delta_{\text{YORP}} = 0.3, 0.4, \text{ and } 0.5$ , as well as a range of  $c_{\text{YORP}}$  and  $\tau_{\text{coll}}$  parameters. Our output included  $P$  and the obliquity  $\gamma$ , both evolving due to the YORP torques.

For our comparison to observation data, we included two sources. The first source was the rotation rate distribution of small asteroids provided in Pravec et al. (2008) (see Fig. 9). They compiled  $P$  for 268 small main-belt and Hungaria asteroids in the diameter range 3–15 km, with a median diameter of 6.5 km. They analyzed the rotation rate distribution of their sample using histograms and found it was essentially flat except for an overabundance of slow rotators. Using a model comparable to the one described here, they concluded that their YORP effect formulation was able to reproduce observations. Another work, Polishook and Brosch (2009), obtained similar results for 77 asteroids with  $D < 5$  km, though they likely did not resolve those with  $P > 24$  h. It is unclear to us whether this stems from observational bias or is a feature of the distribution. We believe these data represent the best available estimate of the rotation rate distribution of small asteroids, though a careful reader will note that none of them include Bennu-sized bodies.

The spin-axis distribution of small main-belt asteroids was taken from the work of Hanuš et al. (2011) (see Fig. 10; see also

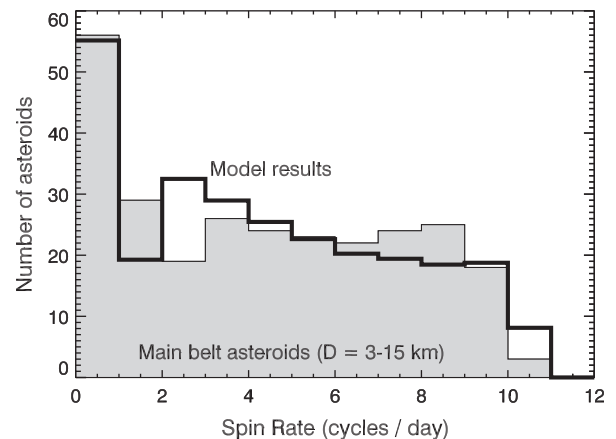


**Fig. 9.** A comparison between the rotation rate distribution of small asteroids from Pravec et al. (2008) and our model results. The dark histogram includes the rotation periods of 268 main-belt and Hungaria asteroids with  $D = 3\text{--}15$  km. The solid line shows our fit for our synthetic km-size asteroids evolving under our static YORP model.

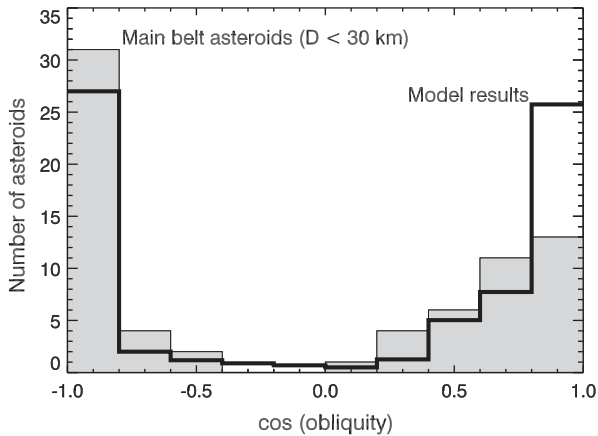


**Fig. 10.** A comparison between the obliquity distribution of small main belt asteroids from Hanuš et al. (2011) and our model results. The gray histogram corresponds to the obliquities of 72 asteroids with  $D < 30$  km. The solid line shows our fit for our model asteroids evolving under our static YORP model.

Hanuš et al., 2013). It is exceedingly arduous to resolve the pole positions for small main belt asteroids, so the data presented by the authors only includes objects with  $D < 30$  km. Still, their Fig. 5 gives us a approximate look at the more limited sub-sample of objects with  $D < 10$  km. They found the pole orientation of these smallest bodies was basically bimodal, with the pole positions close to the north and south ecliptic poles. As one moves to larger diameters, the obliquities spread somewhat to lower latitudes. Hanuš et al. (2011, 2013) concluded that their findings were compatible with a sample of objects that evolved due to the YORP effect.

Overall, we found the static YORP model does a good job of matching the observed parameters found in Figs. 9 and 10. Still, we do find a small but noticeable dependence on our input parameters. We find that low values of  $c_{\text{YORP}}$  (i.e., the YORP effect works more slowly, and YORP cycles take place less often) and  $c_{\text{reorient}}$  (i.e., reorientation events occur quickly once very slow rotation is achieved) prevent us from reproducing the overabundance of the slow rotators found in the left most bin of Fig. 9. On the other hand, nominal values of unity for both parameters yield too many slowly-rotating bodies. Our experience is that  $c_{\text{reorient}} \geq 1$  creates an overabundance of slowly-rotating asteroids that is not observed. Large values of  $c_{\text{YORP}}$  (i.e., a strong YORP effect, and lots of YORP cycles) with low values of  $c_{\text{reorient}}$  (i.e., reorientation events occur quickly once slow rotation is achieved) tends to push too many objects to extreme obliquity values of  $0^\circ$  or  $180^\circ$ , though we caution the data could be misleading. Recall that we are trying to fit to the data for  $D < 30$  km, while our model asteroids have  $D = 1$  km. It could be that we should really be trying to fit our results to the more extreme obliquities in the  $D < 10$  km data, where we unfortunately have little data.

The best match for a steady-state distribution of rotation rates and obliquities between our model asteroids and observations (Figs. 9 and 10) yields parameters near  $\delta_{\text{YORP}} = 0.4$ ,  $c_{\text{reorient}} = 0.9$ , and  $c_{\text{YORP}} = 0.5\text{--}0.7$ , in agreement with the modeling work in Hanuš et al. (2013). This suggests we need YORP to be a little weaker than the nominal values (value of unity), with more time between YORP cycles. We also need collisional reorientation events for our model asteroids to take a little longer once a slow spin state is reached than our nominal case.

We infer the following from our results.

- Our best fit  $\delta_{\text{YORP}}$  value of  $\approx 0.4$  indicates there is a small preference for spinning down vs. spinning up when it comes to small asteroids. This is not surprising, because the main feature of the

rotation-rate distribution we seek to match is an overabundance of the slow rotators (Fig. 9). Note, however, that Pravec et al. (2008) matched the same results using a different approach to model this population. They assumed the rotation-rate evolution “effectively slows down” for periods longer than 24 h with  $\delta_{\text{YORP}} = 0.5$ . They justified their point of view by effectively capturing the onset of tumbling as well as how the model asteroid reemerges from this state. Regardless, both approaches are empirical at this stage of model development and both should be used with some caution.

- Our best fit YORP effect parameter of  $c_{\text{YORP}} = 0.5\text{--}0.7$  is slightly weaker than the nominal cases, supporting the results of Rozitis and Green (2012) and in accordance with findings by Hanuš et al. (2013).
- As for  $c_{\text{reorient}}$ , Bottke et al. (2005) showed in their Fig. 14 that the size distribution of small main-belt asteroids is steep enough that their derived disruption timescale for  $D = 0.01\text{--}1$  km bodies was slightly smaller than that derived by Farinella et al. (1998). Given the similarities in the intrinsic calculation, we expect comparable results for  $\tau_{\text{coll}}$  as well.

Using our Monte Carlo code with these refined parameters, we can test our procedure by reconstructing the  $N(C)$  distribution for the Erigone family. This task has already been performed in detail by Vokrouhlický et al. (2006a), so here we merely verify the performance of our code with the new parameters, namely  $\delta_{\text{YORP}} = 0.4$ ,  $c_{\text{reorient}} = 0.9$ , and  $c_{\text{YORP}} = 0.7$ . Even so, we found something interesting in the process of our modeling work.

Using the same initial conditions as in Vokrouhlický et al. (2006a), we downloaded the latest estimate of the family from the PDS node (Nesvorný, 2012; see also Fig. 4, we only trimmed the suspected interlopers far below the V-shape lines from our analysis). To make our run comparable with our favored Eulalia-family runs below, we chose surface thermal conductivity values of  $K = 0.03$  W/m/K, thermal capacity  $C_p = 800$  J/kg/K, and surface and bulk densities of  $1$  g/cm<sup>3</sup>. This choice implies surface thermal inertia  $\approx 150$  J m<sup>-2</sup> s<sup>-1/2</sup> K<sup>-1</sup>, appropriate for  $\sim 5\text{--}10$  km asteroids (e.g., Delbò et al., 2007). Their initial pole orientation was random in space and  $P$  values were assigned according to a Maxwellian distribution with a peak at 8 h.

According to our best fit case, the age was  $130^{+25}_{-10}$  Myr for the Erigone family. This is in apparent discordance with the age  $>250$  Myr inferred by Vokrouhlický et al. (2006a), in spite of the overall agreement of a rather young age. A small portion of this difference can be attributed to the thermal conductivities used: Vokrouhlický et al. use log-random values between 0.005 and 0.05 W/m/K, while we use  $K = 0.03$  W/m/K. Higher conductivities values lead to slower Yarkovsky drift and older ages. The biggest factor, however, is the bulk density used in Vokrouhlický et al. (2006a) was  $2.5$  g cm<sup>-3</sup>, a high value for a C-type asteroid (i.e., Mathilde and Bennu have bulk densities of  $1.3$  g cm<sup>-3</sup>, respectively; Britt et al., 2002; Chesley et al., 2014). For this test case, we choose a value of  $1$  g cm<sup>-3</sup>, with lower bulk densities decreasing the mass of the model asteroids and making Yarkovsky drift and YORP evolution faster (and thus the age lower). This lower age is an important part of our story for the origin of Bennu.

### 5.3. Using the Static YORP model to fit the Eulalia family

Using our calibrated static YORP model (i.e., the body’s  $c_{\text{YORP}}$  and shape parameters are held constant until a YORP endstate is reached), we can now try to compare our model results with older, more spread out families like Eulalia and New Polana with ear-like structure (Figs. 6 and 7). To do so, however, we need to consider some additional complications in more detail.

First, a good share of the original Eulalia family has been eliminated by the J3:1 resonance (Walsh et al., 2013). We estimate that about half of the initial family members were directly injected into the J3:1 by the family-forming event, where they were readily pushed into the planet-crossing region. Of the remainder, which were thrown in the opposite direction of the J3:1 boundary, roughly half were given initial obliquity values that were positive. This means most of these objects drifted outward by Yarkovsky effect until they too entered the J3:1 resonance. Accounting for this attrition, this would only leave about 25% of the original objects in the Eulalia family. We account for this process explicitly in our runs by assuming all objects that reach 2.5 AU are discarded.

Second, the  $N(C)$  distribution of the Eulalia-family has a large evacuated center near  $a_c$  and a curious displaced ear compared to other families analyzed in previous works (Fig. 11). As an example, consider the differences between Eulalia's  $N(C)$  distribution (solid dots) and that of the comparably-aged Eos family shown in Fig. 12 of Vokrouhlický et al. (2006c). The  $N(C)$  distribution is more unusual here, partly because we are looking at different-size objects, but also because the Eulalia family formed on the brink of the J3:1, where objects undergoing a random walk in semimajor axis can easily be eliminated.

In our model runs, we first attempted to fit the  $N(C)$  distribution over a matrix of values of evolution time  $T$  and mean Gaussian velocity  $V$  with which the  $D = 5$  km Eulalia family members were spread after the breakup (see definition of  $V$  above). We found that for bulk density  $1.5$  g/cm<sup>3</sup>, surface conductivity  $0.03$  W/m/K, our best fit age was  $1440$  Myr and the initial velocity field  $V = 20$  m/s. For the same parameters, but bulk densities of  $1$  g/cm<sup>3</sup>, we obtained an age of  $960$  Myr. These results are consistent with simply rescaling things using the preferred density. The formal age and velocity uncertainties are  $\approx \pm 100$  Myr and  $10$  m/s, respectively, for both runs.

As Fig. 11 shows, though, our best fit cases with the static YORP model are only modestly successful, both as viewed by eye and using  $\chi^2$  tests. The bodies used in the fit are large enough that most have experienced less than one YORP cycle. The long tail of  $N(C)$  values near the  $C = 0$  value comes from the loss of  $a \geq 2.5$  AU bodies via the J3:1.

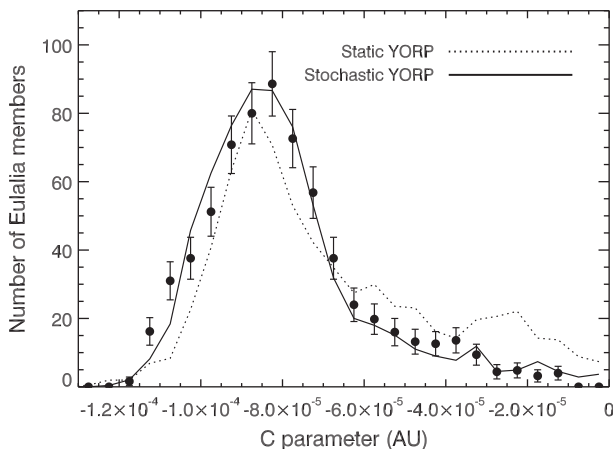


**Fig. 11.** A comparison between the static and stochastic YORP models. The solid points are the  $N(C)$  distribution values of the Eulalia family for  $H < 16.5$  taken from Fig. 8. The error bars assume standard square root values. The dashed line corresponds to our static YORP model results, while the solid line is for our stochastic YORP model. Here we assumed bulk density  $1$  g/cm<sup>3</sup> and surface conductivity  $0.03$  W/m/K. The runs yielded an age of  $960$  and  $830$  Ma for the static and stochastic YORP models, respectively. Their initial velocity fields were characterized by  $V = 20$  m/s and  $V = 40$  m/s, respectively. Note the long low tail on the right side of the plot. This corresponds to the loss of objects through the J3:1 resonance.

More obvious problems are observed when we track smaller Eulalia family members that should have experienced multiple YORP cycles. To demonstrate this, as well as provide insights into the delivery of Bennu-like members to the  $\nu_6$  resonance, we conducted the following test simulations. We started  $5$  million Eulalia members at the exact location of the family center at  $a_0 = 2.493$  AU (to simplify our analysis, we assumed  $V = 0$  km/s for these specific runs). The model asteroids were assigned  $11.8 < H < 22$  and albedos of  $p_V = 0.05$ . The surface conductivity and bulk density of each body was set to  $0.03$  W/m/K and  $1$  g/cm<sup>3</sup>, respectively. We also set two termination boundaries in semimajor axis: (i) the J3:1 resonance at  $2.5$  AU, and (ii) the  $\nu_6$  resonance estimated at  $2.14$  AU for the few degree inclination orbits appropriate for the Eulalia family. Whenever an asteroid reached those values, it was eliminated from the simulation. For the moment, we ignored the effects of the J7:2/M5:9 resonance.

Nine snapshots of our semimajor axis evolution results for model Eulalia family members are shown in Fig. 12. The sizes of the bodies were set to  $D = 0.5$  km (Bennu-sized),  $1.8$  km, and  $3.4$  km, and their semimajor axis values were recorded at evolution times  $T = 0.1$  Gyr,  $0.5$  Gyr, and  $1$  Gyr. The number of bodies in each snapshot, represented by a histogram, was divided by the number of particles in the  $0.1$  Gyr timestep. The location of the 75 percentile of the surviving bodies at the timestep was marked with a solid line; 25% of the particles are to the left of the line (in white), and 75% are to the right of the line (in gray). The smallest objects were placed in the top row of the figure to mimic their placement in the family ( $a, H$ ) plots (Fig. 4).

The snapshots for  $D = 1.8$  and  $3.4$  km at  $T = 0.1$  Gyr display how the ear in the Eulalia family was produced. Many of the objects had their obliquities moved to  $180^\circ$  by YORP torques, giving them the maximum possible inward drift rate ( $da/dt$ ) by the Yarkovsky effect. The smaller objects also drift faster than the bigger objects, giving them a bigger spread in semimajor axis. The top left snapshot, for Bennu-sized objects at  $D = 0.5$  km and  $T = 0.1$  Gyr, however, shows only the tiniest remnant of an ear at  $a < 2.4$  AU. The reason is that YORP cycles have caused many objects to undergo multiple spin axis reorientation events, which in turn has caused their  $da/dt$  values to potentially flip signs again and again. This random walk leaves in its wake a Gaussian-shaped distribution, and it is the telltale sign of a population that has experienced numerous YORP cycles.

The remaining snapshots show how the semimajor axis distributions of the larger bodies slowly change into Gaussian-like shapes as more bodies undergo YORP cycles. The ears of each population slowly fade as more objects in this wavefront have their drift direction reversed. Eventually, at  $T = 1$  Gyr, all but the  $D = 3.4$  km bodies have lost their signature of the ear altogether. The net number of bodies in the distributions also decreases with time as objects random walk their way into the J3:1 resonance at  $2.5$  AU. For the Bennu-sized  $D = 0.5$  km bodies, only a small fraction make their way across the inner main belt to the  $\nu_6$  resonance (at  $2.14$  AU) in  $1$  Gyr.

We are now ready to compare and interpret our static YORP model results against the observed Eulalia family (Fig. 13; see also Fig. 6). The solid lines show the 75th percentile marks of our model asteroid distributions as defined in Fig. 12. The dashed lines show the location of the fastest objects in our distribution. When they reach  $2.14$  AU, it indicates some bodies have escaped the main belt through the  $\nu_6$  resonance.

The curvature of the 75 percentile lines show that small asteroids (e.g., those with  $H < 17$ , or  $D \sim 2.2$  km) break away from the classical V-shape curves at ages  $0.5$  Gyr. As time goes on, larger bodies also become discordant with the observed distribution of the Eulalia family's ear. Using Fig. 12, we can now explain this behavior as the byproduct of YORP cycles producing a random

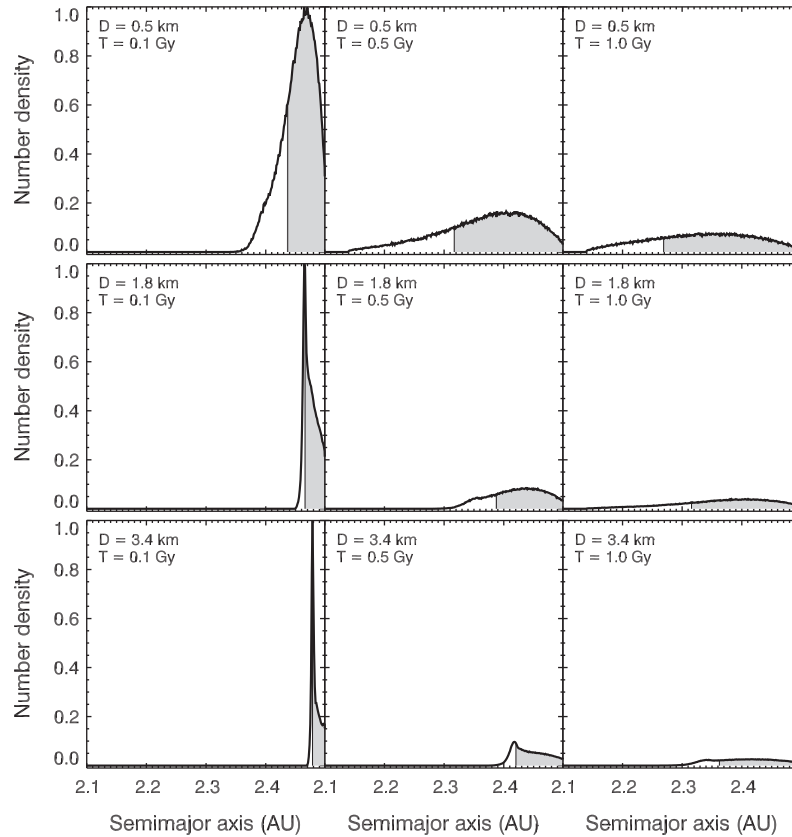


**Fig. 12.** Nine snapshots our model asteroids evolving inward from the Eulalia family within our static YORP model runs. We started with  $5 \times 10^6$  asteroids at the semimajor axis location of (495) Eulalia ( $a = 2.487$  AU). The asteroid sizes were set to  $D = 0.5, 1.8,$  and  $3.4$  km. The snapshots are at 0.1, 0.5, and 1 Gyr. The gray histogram corresponds to the location where 75% of the simulation's asteroids are located in the distribution. The  $\nu_6$  and J3:1 resonances are located at 2.14 and 2.5 AU; objects reaching either are removed. The sharp spikes in the distribution show the location of the family's ear. YORP torques have modified their obliquities to  $\sim 180^\circ$ , and the bodies have yet to undergo YORP cycles. The Gaussian-like patterns are caused when many bodies reach YORP endstates, which allow them to change the sign and magnitude of their direction ( $da/dt$ ). These so-called YORP cycles eventually eliminate the family's ears.

walk in the semimajor axis migration of these bodies. As the distribution moves to an increasingly Gaussian-like shape, the bodies lose their ability to preserve the Eulalia family's ear. For reference, the estimated YORP-cycle timescale for  $D \sim 2.2$  km bodies is  $\leq 50$ –100 Myr, such that the  $> 0.5$  Gyr ages represent numerous YORP cycles for each body. These results also explain why the  $N(C)$  fits in Fig. 11 are inaccurate for the static YORP model case.

In an attempt to get better agreement between model and data, we experimented with various ejection velocities ( $V$  values) and even some size-dependent ejection velocities, despite evidence to the contrary from the orbits of young observed families. Unfortunately, these trials tended to fail outright or they required us to use unrealistically large and/or ad hoc initial velocity fields. None provided a satisfying solution.

This left us with a conundrum. The static YORP model can reproduce the rotation rate and obliquity constraints provided by small asteroids while also matching the  $N(C)$  distribution of young families like Erigone (i.e., a family where the largest bodies have not experienced many YORP cycles). For older, spread-out families like Eulalia, however, our static YORP model fails because YORP cycles produce a random walk for small bodies in semimajor axis. The mismatch seen in Fig. 13 strongly suggests we are missing a key YORP component, one that probably linked to the nature and timing of YORP cycles.

#### 5.4. The Stochastic YORP model and the Eulalia family

In order to understand what we might be missing, we further examined the details of the Eulalia family. For example, when

Walsh et al. (2013) was comparing its  $(a, H)$  distribution with the “canonical V-shape curves”, they found they needed two values of the best-fit  $C$  parameter to match the family boundary: (i)  $C = 10.5 \times 10^{-5}$  AU for the large bodies with  $H \leq 15$ , and (ii)  $C = 9.2 \times 10^{-5}$  AU for the smaller bodies with  $H \geq 16$ . Put in more plain language, using the  $C$ -parameter as a measuring stick, the semimajor axis distance between the family ear and the family center ( $a_0$ ) is less for smaller family members than it is for larger family members (i.e., the small objects traveled slightly slower than one would expect based on the drift rates of the larger objects).

The observation that the family is basically bound by one of the V-shape curves, though a slight brake was applied to the mobility of smaller family members, was puzzling to us. It combined the behavior of the larger bodies with a milder version of the YORP cycle-driven random-walk effects. Given our static YORP's model ability to match numerous observational constraints, we suspected the problem might be in how we were defining YORP cycles. This led us to implement new YORP physics into our code that has only recently been discovered by Statler (2009). Adopting his terminology, we refer to this as the *stochastic YORP* model.

Statler (2009) used numerical simulations to investigate how tiny changes in topography, such as the formation of a small crater or even the movement of a boulder from one place to another, could modify the YORP torques. These small-scale irregularities on an asteroid's surface can sometimes translate into dramatic changes to the magnitude and sign of the change in rotation rate. His work shows that we can no longer assume the torque acting on the rotation rate is fixed between YORP endstates, but instead

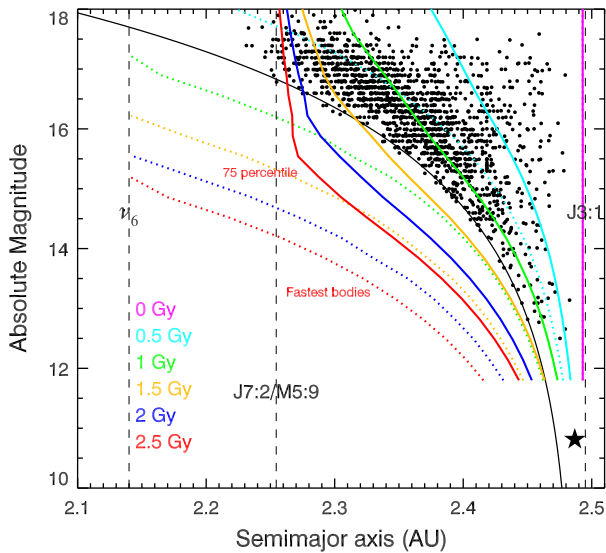


**Fig. 13.** Application of the static YORP model to the Eulalia family. We started  $5 \times 10^6$  Eulalia members at the semimajor axis location of (495) Eulalia ( $a_0 = 2.493$  AU; see filled star). Thus, all bodies were assigned  $V = 0$  m/s. The sizes of the model asteroids were evenly distributed between  $11.8 < H < 22$  and were given albedos of  $p_V = 0.05$ , surface thermal conductivity values of  $K = 0.03$  W/m/K, thermal capacity  $C_p = 800$  J/kg/K, and surface and bulk densities of  $1$  g/cm $^3$ . Their initial pole orientation was random in space and  $P$  values were assigned according to a Maxwellian distribution with a peak at 6 h. We assumed that  $\delta_{\text{YORP}} = 0.5$ ,  $C_{\text{reorient}} = 0.9$ , and  $C_{\text{YORP}} = 0.7$ . Two termination boundaries were set in semimajor axis: the first at the J3:1 resonance at 2.5 AU, and second at the  $v_6$  resonance at 2.14 AU. When asteroids reach these boundaries, they were removed from the simulation. The colors represent elapsed time in the simulations. The dashed lines are the fastest bodies, while the solid lines are the 75 percentile as defined in Fig. 12. Our static YORP model does not do a good job of fitting the ear of the Eulalia family. The fact that most  $H > 16$  objects have traveled a comparable distance from  $a_0$  at any given time is explained by the effect of YORP cycles, which causes obliquity (and Yarkovsky drift rate direction) to undergo a random walk.

must vary, perhaps frequently, while the asteroid's spin rate evolves.

The driver for shape changes could be cratering events or the steady addition or subtraction of rotational angular momentum by YORP. For the latter, consider that as a body spins up, components will try to act like a spinning figure skater's arms; they will expand outward in a radial direction if they can overcome friction. This may lead to downslope movement and eventually mass shedding (e.g., Walsh et al., 2012a). The bottom line here is that, unlike in the case of the Yarkovsky effect, small-scale irregularities in an asteroid's shape affect the strength of the YORP effect in meaningful ways.

Hints of the consequences of the Statler (2009) conclusions can be traced back to the examination of the YORP effect on the peculiarly-shaped asteroid (25143) Itokawa by Scheeres et al. (2007), later revisited in somewhat more detail by Breiter et al. (2009). Analytical studies of the YORP effect by Nesvorný and Vokrouhlický (2006) as well as Breiter and Michałska (2008) suggest similar consequences, namely that high multipoles in spherical-harmonic shape representations play a key role in YORP strength.

To include these effects, we had to make different assumptions about how the YORP torques are handled. In the current model, YORP torques were calculated for hundreds of asteroid shape models, with the resulting torques represented in a functional form that followed a Gaussian distribution (see Čapek and Vokrouhlický, 2004). When a model asteroid is included within a simulation, a torque solution was randomly chosen from this distribution, with

the torque fixed until the model asteroid reached a YORP endstate. Only then was a new torque solution selected.

In the new stochastic YORP formulation, a different torque solution is chosen every time the timescale  $\tau_{\text{YORP}}(D)$  is exceeded (see Appendix A). The length of  $\tau_{\text{YORP}}(D)$  is unknown to us at present, and we suspect it may vary from one asteroid shape to the other. After testing various values, we settled on an assumed  $\tau_{\text{YORP}}(D)$  that is a factor >10 times smaller than the YORP cycle timescale for our model asteroids. As we will discuss below, this choice provides good fits to the observed Eulalia and New Polana family data in  $(a, H)$ . It is also consistent with numerical results describing how rubble-pile asteroids change shape in response to an increase/decrease in rotational angular momentum via the YORP effect (see Cotto-Figueroa, 2013, submitted for publication; Statler, 2014, personal communication).

Intriguingly, stochastic YORP behavior does not appear to affect the evolution of an asteroid's obliquity by YORP torques. This means the evolution of objects toward  $0^\circ$  and  $180^\circ$  should continue as in the static YORP case (see Appendix A). This allows our new model results to fit the same primary constraints as the static YORP model.

Using our stochastic YORP model, we now reexamine the Eulalia family. Fig. 11 shows our best-fit  $N(C)$  distribution for the same model asteroids selected previously (i.e., bulk density of  $1$  g/cm $^3$ ,  $p_V = 0.05$ , surface conductivity  $0.03$  W/m/K). We set  $\tau_{\text{YORP}}$  to be 1 Myr for the observed objects, though no major differences were seen for 0.5 Myr or 2 Myr. The integration timestep for these runs was 0.2 Myr. The initial velocity field remains low ( $V \approx 40$  m/s with about 10 m/s uncertainty).

As an aside, we provide some additional arguments justifying  $\tau_{\text{YORP}} \approx 1$  Myr based solely on cratering rates. The characteristic size of Eulalia asteroids in Fig. 11 is between 4 and 8 km diameter. The population of  $D > 20$  m impactors in the main belt is  $\sim 10^{11}$  (e.g., Bottke et al., 2005a,b). Given an intrinsic collision probability of  $\sim 3 \times 10^{-18}$  km $^{-2}$  y $^{-1}$ , we expect one such sub-catastrophic impact occurs every  $\sim 150$  ky, and that it produces a  $\sim 200$  m crater. If 6–10 such events are enough to significantly change the shape of the body to redefine the YORP strength, we obtain a 1 Myr timescale for  $\tau_{\text{YORP}}$ . This value is much shorter than the estimated YORP-cycle timescale for  $D = 4$ –8 km bodies.

Our new age for Eulalia is 830 Myr, with an uncertainty of 100 Myr. The best-fit  $N(C)$  values also match observations by eye and using  $\chi^2$  tests, though a few small inconsistencies remain. It should be noted that the 100 Myr uncertainty is a formal one. Varying more parameters, such as the surface thermal conductivity, would change the solution and increase the age uncertainty. We note that admissible solutions will then extend toward larger ages. Without performing a comprehensive search in the available parameter space, we predict the Eulalia age should be conservatively taken as  $0.83^{+0.37}_{-0.10}$  Gyr. It is also important to consider that the bulk density assumed,  $\rho_{\text{bulk}} = 1$  g cm $^{-3}$ , will also affect the results. Modifying the bulk density means we would potentially need to modify the family's age according to the  $\propto \rho_{\text{bulk}}$  rule.

The ears of our semimajor axis for  $D = 0.5, 1.8,$  and  $3.4$  km also now last longer than in the static YORP case. Consider Fig. 14, the stochastic YORP counterpart to Fig. 12. We see each inward moving ear is sharper in our 9 snapshots, and the onset of the random walk caused by YORP cycles is held off longer. This produces a larger spread of bodies in semimajor axis at each timestep.

There is also considerable improvement in our Eulalia family fits using our ensemble of  $11.8 < H < 22$  bodies. Compare our results for Fig. 15, which use the stochastic YORP model, with the static YORP results for Fig. 13. We find the 0.5 and 1 Gyr wavefronts mimic the general shape of the V-shaped Yarkovsky line until  $H > 17.5$  or so, where the 75 percentile line begins to change shape on account

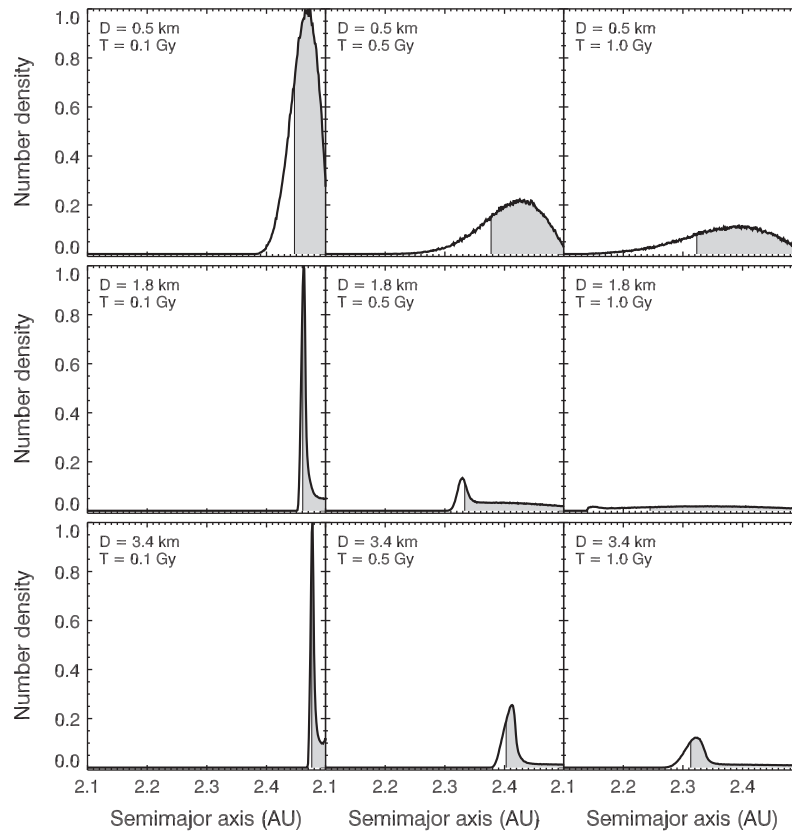


**Fig. 14.** Nine snapshots our model asteroids evolving inward from the Eulalia family within our stochastic YORP model runs. The asteroid sizes were set to  $D = 0.5, 1.8,$  and  $3.4$  km, and the times shown are 0.1, 0.5, and 1 Gy. Starting conditions and format are the same as Fig. 12. Compared to the static YORP case shown in Fig. 12, we see the family's ears persist for a much longer period of time.

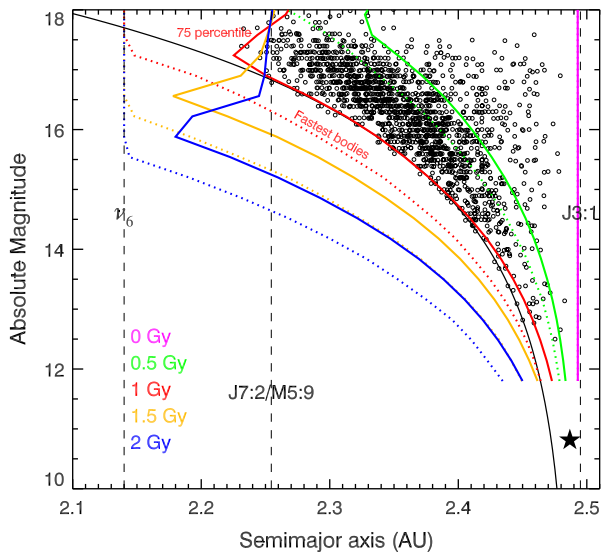


**Fig. 15.** Application of the stochastic YORP model to the Eulalia family. For this test run, initial conditions and labels are described in the caption of Fig. 13. Here we see that the 75 percentile, as defined in Fig. 12, does a good job at reproducing the shape of the family's ear. The small objects in the family cross the main belt much more quickly than in our static YORP model (Fig. 13) because only the spin rates of the model asteroids undergo a random walk, not the obliquities. The unusual turnaround in the curves on the left side is a byproduct of two factors: small objects leave the main belt through the  $v_6$  resonance, and YORP cycles produce a random walk in semimajor axis among the bodies left behind.

of the depletion of material exiting the  $v_6$  resonance. Note that the location of the  $J7:2/M5:9$  resonance is shown here for reference, but our simulation did not allow objects to interact with it.

Overall, the stochastic YORP model keeps asteroids away from YORP endstates longer, and therefore it helps the bodies move across the main belt faster than before. We believe it provides a physically reasonable solution to the mismatches found between the static YORP model results and the Eulalia family. We will now employ the stochastic YORP model to simulate the evolution of all of low albedo candidate families.

## 6. Family results

### 6.1. Calculating the ages of our low albedo inner main belt families

With our stochastic YORP model tested, we are now ready to track the evolution of our dark, low-inclination inner main belt families that could have plausibly produced Bennu (see Fig. 3). Our immediate goal will be to estimate the age of each family. If the family age proves to be less than the interval needed for Bennu-sized bodies in the family to escape the main belt via the  $v_6$  or  $J7:2/M5:9$  resonances, we can rule out that family as a source. Note that our age determination method here will be more approximate than our previously used  $N(C)$  method. This is because the New Polana, Clarissa, and Sulamitis families lack sufficient coverage of their larger asteroids to apply this technique. For reference, our model asteroids were given  $p_V = 0.05$ , surface conductivities of  $0.03$  W/m/K, and bulk densities of  $1$  g/cm<sup>3</sup>.

### 6.1.1. Ejection velocities from families

An issue that could strongly affect our results concerns the initial velocity spread of Bennu-sized fragments from each candidate family. Estimates suggest that every 100 m/s of ejection velocity translates into a semimajor axis change of up to 0.025 AU for Bennu-sized bodies. This represents the equivalent of  $\sim 100$  Myr of Yarkovsky evolution. Not surprisingly, if a high enough ejection velocity was selected, nearly any low albedo family across the main belt could potentially produce Bennu.

To better constrain this issue, we carefully examined what is known of the ejection velocity distributions of young asteroid families, especially those that have not had time to evolve substantially by the Yarkovsky effect. Recall that a family member's orbit after a cratering or catastrophic disruption event is the vector sum of the parent body's velocity around the Sun combined with the fragment's ejection velocity. This combination must exceed the escape velocity of the parent body. Interestingly, when we calculate the relative velocity of the orbits of family members in a young family to that of the largest remnant, the relative velocity obtained is always comparable to or less than the approximate escape velocity of the parent asteroid. This means the ejection velocities of most sizable family members is likely to be low.

As examples, consider four very young families. The observed family members of the 5.8 Myr old Karin family have a maximum orbital relative velocity, compared to the largest remnant of the Karin family, of about 15 m/s (Nesvorný et al., 2002c, 2006b; Nesvorný and Bottke, 2004). This value is consistent with the estimated parent body diameter derived for the Karin family, 25–30 km, and an escape velocity of 12–15 m/s. Similarly, the 0.5 Myr, 6.9 and 8.3 Myr old Datura, Theobalda, and Veritas families have members that show a maximum relative velocity compared to the largest remnant of 5, 35–40, and 35–40 m/s, respectively. These values are again comparable to the parent body's escape velocity, assuming these parent bodies were  $\sim 10$  km,  $\sim 80$  km, and 80–160 km in diameter, respectively (e.g., Nesvorný et al., 2003; Nesvorný et al., 2006a; Tsiganis et al., 2007; Vokrouhlický et al., 2009; Novaković, 2010).

It is also useful to consider the ejected fragments from (4) Vesta, whose members may be dominated by ejecta from the massive Rheasilvia and Venenia basin-forming events  $\sim 1$  and  $>2$  Gyr ago, respectively (Marchi et al., 2012). Numerical tests suggest that Vesta family members in the inner main belt are  $<370$  m/s away from Vesta itself. The family members have similar inclinations to Vesta itself, and they span the entire distance between the  $\nu_6$  and J3:1 resonances. No concentration of V-type fragments with similar inclinations to Vesta has yet been found on the far side of the J3:1 resonance ( $a > 2.5$  AU) adjacent to the J3:1 boundary (e.g., Roig and Gil-Hutton, 2006; see also Carruba et al., 2014), as would be expected if these bodies were produced over the last few Gyr as Vesta ejecta. As before, these relative velocities are found to be consistent with Vesta's escape velocity ( $\sim 360$  m/s; Russell et al., 2012).

Accordingly, in the runs below, we limit the ejection velocities so the relative velocities of the smaller bodies compared to the largest remnant do not exceed the approximate escape velocity of the parent asteroid.

### 6.1.2. Eulalia family

We first investigate the Eulalia family (Fig. 16). Here we used  $V = 40$  m/s for the  $D = 5$  km asteroids; recall that smaller asteroids have larger ejection velocities, as discussed above and in Vokrouhlický et al. (2006a). We set a maximum velocity for our smallest fragments of 100 m/s. We could easily justify a smaller velocity, say one between 50 and 80 m/s for a parent body size of 100–160 km diameter, but we decided to go a little beyond this limit to err on the side of caution for bodies smaller than the main

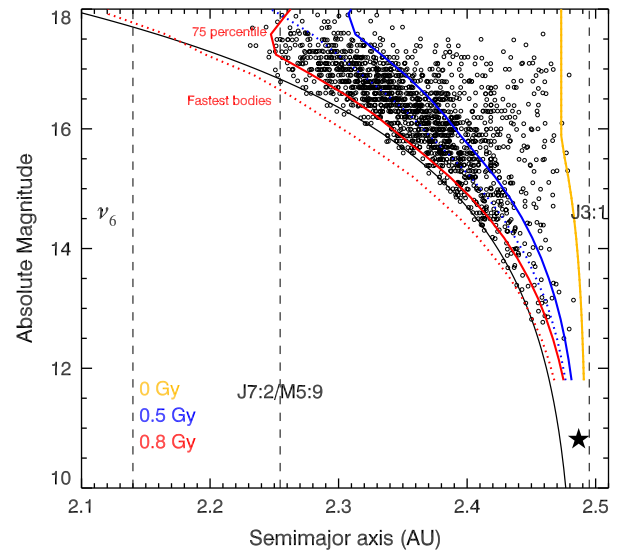


**Fig. 16.** Modeling the age of the Eulalia family using the stochastic YORP model. The initial conditions and labels are described in Figs. 6 and 13. One difference is that we assume an ejection velocity  $V = 30$  m/s for the  $D = 5$  km asteroids, with the smaller asteroids having higher velocities as discussed in the main text and Vokrouhlický et al. (2006a). We set a maximum velocity for our smallest fragments of 150 m/s. The 75 percentile, as defined in Fig. 12, is set to match the break in the family's shape away from the standard V-shaped line for  $a < 2.3$  AU. We estimate that the approximate age of the family is  $0.8 \pm 0.1$  Gyr.

belt observational limit. This difference only slightly affects our results.

Note that the 75 percentile wavefront is at  $\approx 0.8$  Ga, the same age determined by the more accurate  $N(C)$  distribution fitting method (Fig. 11). The curve follows the precise shape of the observed family's ear, particularly where small family members move away slightly from the V-shaped curve at  $H > 16$ .

### 6.1.3. New Polana family

The New Polana family has limited data, and fits to  $N(C)$  are more problematic to apply given the heavy depletion in the family. Instead, we apply our stochastic YORP model in  $(a, H)$  space to determine an approximate age (Fig. 17). We estimate that New Polana is  $1.4 \pm 0.15$  Ga. The error bar here is a formal one; modifications to asteroid parameters, such as the surface thermal conductivity, could increase the age by several hundreds of Myr. The 75 percentile wavefront for  $H > 16.5$  also has an odd shape, partly because YORP cycles produce a random walk in semimajor axis distribution of the bodies, but also because many fast moving bodies have already been eliminated by reaching the  $\nu_6$  resonance.

### 6.1.4. Erigone family

Our stochastic YORP runs for the Erigone family are shown in Fig. 18. The family is quite young; we predict a model age of 130 Myr with an uncertainty of a few tens of Myr. We used a smaller ejection velocity  $V$  for this family of 30 m/s, with a maximum of 50 m/s for the smaller bodies. The parent body's size has been estimated to be  $D \sim 110$  km (e.g., Durda et al., 2007). The observed family members have not spread enough to undergo many YORP cycles. This explains why our static and stochastic YORP models yield similar ages.

Our runs suggest few Bennu-sized Erigone family members have reached the J7:2/M5:9 or the  $\nu_6$  resonance at 130 Myr. Still, for some Erigone family members, there may be other ways out of the main belt (see also Campins et al., 2013). Of all of the dark families investigated here, Erigone family members have the largest mean proper eccentricity (Fig. 3). Using our numerical integra-

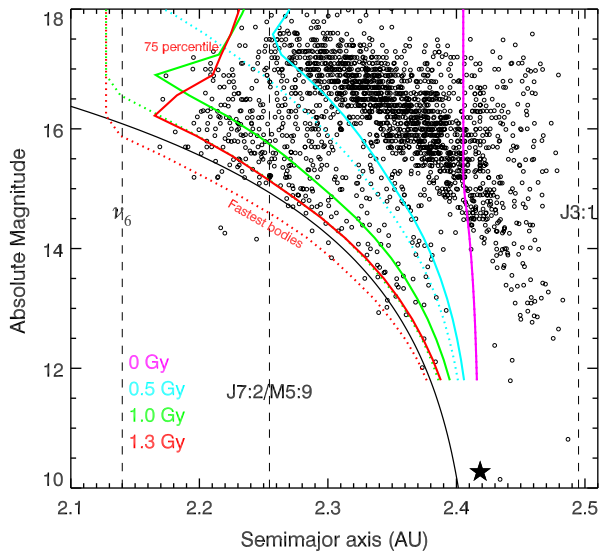


**Fig. 17.** Modeling the age of the New Polana family using the stochastic YORP model. The Eulalia family is also shown. The initial conditions and labels are described in the caption of Figs. 7 and 13. We assume an ejection velocity  $V = 30$  m/s for the  $D = 5$  km asteroids, with the smaller asteroids having higher velocities as discussed in the main text and Vokrouhlický et al. (2006a). We set a maximum velocity for our smallest fragments of 100 m/s. The 75 percentile, as defined in Fig. 12, suggests the family's age is approximately  $1.4 \pm 0.15$  Ga.

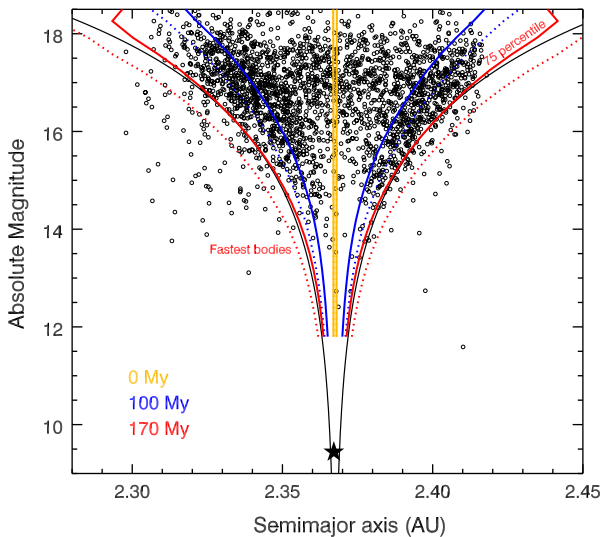


**Fig. 18.** Modeling the age of the Erigone family using the stochastic YORP model. The initial conditions and labels are described in the caption of Figs. 4 and 13. We assume an ejection velocity  $V = 30$  m/s for the  $D = 5$  km asteroids, with the smaller asteroids having higher velocities as discussed in the main text and Vokrouhlický et al. (2006a). We set a maximum velocity for our smallest fragments of 150 m/s. The 75 percentile, as defined in Fig. 12, suggests the family's age is approximately 170 Myr, with a more formal age coming in at  $170_{-30}^{+25}$  Myr from our static YORP model (see text).

tion code from Section 3, we tracked a population of 668 test asteroids with  $D = 0.5$  km, assuming their initial orbits mimicked those that make up the approximate starting orbits of Erigone's inner ear (with  $a < 2.367$  AU). We assumed these bodies had the maximum inward Yarkovsky drift rates suitable for a  $D = 0.5$  km body. Our results showed that at  $\sim 100$  Myr, secular perturbations pushed 10–20% of these asteroids, namely those with the highest eccentricities, into the IMC region near  $a = 2.25$ – $2.3$  AU. Interestingly, nearly all of these bodies lingered near the Mars-crossing line until

130 Myr. Only 3% of the entire population achieved Earth-crossing orbits by 130 Myr through a combination of Mars encounters and resonances. None of the test asteroids reached Bennu-like orbits before 130 Myr.

These results suggest that the Erigone family is an unlikely source for Bennu when compared to the alternatives, in agreement with Campins et al. (2013). Despite this, it is possible that Erigone is an important source of sub-0.5 km low albedo NEOs and meteoroids; their higher Yarkovsky drift rates may allow some of them to reach the terrestrial planet region and Earth within the last 130 Myr. A comparison between sub-0.5 km low albedo NEOs and the spectra of Erigone family members might potentially yield interesting results in the future.

#### 6.1.5. Sulamitis and Clarissa families

A full dynamical workup of the Sulamitis and Clarissa families is unnecessary if our goal is to determine whether it was a likely source for Bennu. The easier way to proceed is to simply compare them to the Erigone family.

As discussed in Section 2, and as seen in Figs. 3–5, the number of known objects in the Sulamitis family implies its parent body was probably similar to or slightly smaller than the Erigone family. In addition, the inward-moving family members of the Sulamitis and Erigone families with  $H < 15$ , defined here as having  $a < 2.463$  AU and  $a < 2.367$  AU, respectively, have a semimajor axis spread of about 0.05 AU from the center of the family. These values imply the families are fairly close in age to one another. Using the left side of the family (members with semimajor axes less than that of the largest remnant (752) Sulamitis), and the  $N(C)$  methods discussed above, we obtained an age of  $200 \pm 40$  Myr, assuming a bulk density for the members of  $1 \text{ g/cm}^3$ . In a similar manner, we estimate the Clarissa family is only  $\sim 60$  Myr.

The Sulamitis and Clarissa families have the lowest mean eccentricities of all of the dark families examined here. This means their inward-evolving family members are unlikely to escape by drifting onto a Mars-crossing orbit. Instead, they probably need to escape via the J7:2/M5:9 or  $\nu_6$  resonances, both which are further away from the Clarissa/Sulamitis families than the Erigone family.

These factors indicate the Sulamitis and Clarissa family members are much less likely to produce Bennu than Erigone family members, which were already poor candidates compared to the alternatives. Thus, by this rationale, we eliminate the Sulamitis and Clarissa family from contention to produce Bennu as well.

#### 6.2. Calculating the likely parent family of Bennu

The work above leaves us with two main candidates to produce Bennu: the Eulalia and New Polana families. Both are in the “sweet spot” in terms of preferred orbital properties, with proper eccentricities between  $0.1 < e < 0.2$  and inclinations between  $3^\circ < i < 4^\circ$  (see Section 2). Both can deliver 0.5 km low albedo objects to the right kinds of orbits within the  $\nu_6$  resonance and the IMC regions (via the J7:2/M5:9 resonance) to produce Bennu. In addition, both families are old enough that they have probably been supplying Bennu-sized bodies to the inner Solar System for some time.

In this circumstance, the family that provides the largest flux to the  $\nu_6$  resonance or IMC regions in the current era is the one most likely to be the source of Bennu from a probability standpoint. This is because the timescale for objects within these sources to reach Bennu's orbit is only a few Myr to a few tens of Myr, short compared to the timescale of major changes to the influx of material reaching the source regions. Our goal in this section is to quantify this probability. We will do this by estimating several factors:

- The net fraction of 0.5 km diameter Bennu-like asteroids from each family that reach the  $\nu_6$  resonance and IMC regions in the current era according to our stochastic YORP model. This value is dependent on the family's formation age.
- The initial size-frequency distribution (SFD) of the families and the quantity of Bennu-sized objects.
- The change in the Bennu-sized population over the family's age in response to collisional evolution, which can serve as both a source and a sink for Bennu-sized bodies via a collisional cascade.
- The probability of a Bennu candidate asteroid within  $\nu_6$  resonance and IMC regions reaching Bennu's orbit.

Each component is discussed below.

### 6.2.1. The flux of dark asteroids that reach likely Bennu escape routes from the main belt

We start with item (a). Here we applied our stochastic YORP model to track the evolution of several sets of  $D = 0.5$  km Bennu-like asteroids within the Eulalia and New Polana families. The initial conditions and asteroid parameters for our runs were described in Section 6.1. The key difference in these runs is that our  $D = 0.5$  km bodies were assumed to have  $\tau_{\text{YORP}} = 0.1$  Myr; this value is  $\sim 10$  times smaller than the YORP cycle timescale.

For each family, we performed two sets of trials, each with 5 million test asteroids. In the first trial, we assumed all bodies reaching the J7:2/M5:9 and J3:1 resonances had their eccentricities increased enough to escape the main belt and reach the NEO population. For the second trial, we assumed the same exit strategy was applicable for bodies that reached the  $\nu_6$  and J3:1 resonances. These results were combined to determine the net flux from each family. In order to compare our results, we plotted the results from the families and escape routes together (Fig. 19).

The origin of the  $x$ -axis in Fig. 19 is defined as the time interval after the family-forming event. The thick solid lines represent the age of each family with error bars: Eulalia being  $0.83^{+0.37}_{-0.10}$  Gyr old

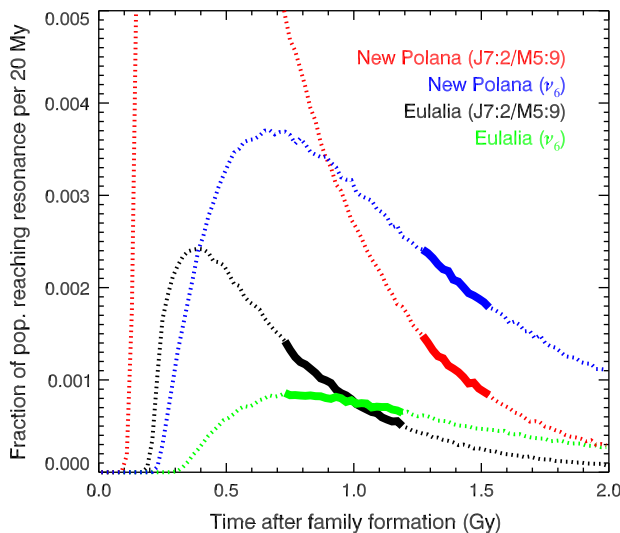


**Fig. 19.** The estimated flux of Bennu-sized bodies ( $D = 0.5$  km) entering the  $\nu_6$  resonance and IMC regions over time from the Eulalia and New Polana families. The  $x$ -axis shows the time since the family-forming event, while the  $y$ -axis is the fraction of the  $5 \times 10^6$  model asteroids that reach the  $\nu_6$  and J7:2/M5:9 resonances per 20 Myr in our stochastic YORP simulations. The  $\tau_{\text{YORP}}$  value here was set to 0.1 Myr. The estimated ages of the families,  $0.83^{+0.3}_{-0.1}$  Ga and  $1.4 \pm 0.15$  Ga, respectively, are shown as thick solid lines. They represent the current flux from those families entering the resonances, and thus can be used to glean insights into the probability that either family made Bennu.

and New Polana being  $1.4^{+0.15}_{-0.15}$  Gyr old. The plots indicate that the flux of Bennu-sized bodies has strongly varied with time. The main surge of Bennu-sized bodies out of the J7:2/M5:9 and  $\nu_6$  resonances was about 0.5–0.7 Gyr after its formation. For Eulalia, the peak flux for the J7:2/M5:9 resonance was  $\sim 0.35$  Gyr after its formation, while its peak flux for the  $\nu_6$  resonance only passed a relatively short time ago.

Here we see that if both families formed simultaneously and were identical in size, the winner of the flux battle over 2 Gyr would be New Polana. At all times, it is comparable to or significantly beats the flux from the Eulalia family. The reason has to do with Eulalia's proximity to the J3:1 resonance; its outward-migrating members do not have to move far to be eliminated. The objects in New Polana's right ear, however, have sufficient space for some to get turned around prior to reaching the J3:1 resonance. This gives the New Polana family a distinct competitive advantage.

The fraction of the starting population from the Eulalia family reaching the  $\nu_6$  and J7:2/M5:9 resonances per 20 Myr in the current era is  $0.83^{+0.03}_{-0.2} \times 10^{-3}$  and  $1.1^{+0.3}_{-0.6} \times 10^{-3}$ , respectively. The same values for the New Polana family are  $2.1^{+0.3}_{-0.3} \times 10^{-3}$  and  $1.1^{+0.2}_{-0.2} \times 10^{-3}$ , respectively. The net flux from each family should be some combination of these values, but calculating the precise value is difficult. We have yet to implement the stochastic YORP model into a numerical integration code that can also account for planetary perturbations. The best we can do at present is to estimate the fraction escaping from each resonance using the numerical integration code discussed in Section 3.

Our results show that about two-thirds of inward drifting bodies started from Eulalia and New Polana will jump across the J7:2/M5:9 on their way to the  $\nu_6$  resonance. This value may underestimate the true value because objects undergoing a random walk in semimajor axis via YORP cycles may encounter the J7:2/M5:9 multiple times on their way to the  $\nu_6$  resonance. On the other hand, YORP cycles may help objects escape long-term trapping within the J7:2/M5:9 resonance. Approximating these effects, we assume here the flux out of the J7:2/M5:9 and  $\nu_6$  resonances is one-third and two-thirds of the total. This places the net flux from Eulalia and New Polana at  $0.9^{+0.12}_{-0.33} \times 10^{-3}$  and  $1.8^{+0.27}_{-0.27} \times 10^{-3}$ , respectively. This suggests that overall, the net flux reaching the  $\nu_6$  resonance and IMC regions from New Polana beats Eulalia by a factor of 1.9, with the range being 1.4–3.5.

For our purposes in finding the probable source of Bennu, however, we only need the ratio of the fluxes from Eulalia to New Polana entering the  $\nu_6$  and IMC regions (with the latter being fed by the J7:2/M5:9). If we define this ratio as  $r_{\text{flux}}$ , we get  $0.40^{+0.08}_{-0.13}$  for the  $\nu_6$  resonance and  $1.0^{+0.56}_{-0.61}$  for the IMC region. The New Polana members dominate the  $\nu_6$  resonance, while both families provide similar fluxes to the IMC region.

### 6.2.2. Estimating the initial size distributions of the Bennu source families

The runs above assume both families start with equal numbers of Bennu-like asteroids. The actual Eulalia and New Polana families, however, may have started out with very different SFD (item b). Consider that not all family-formation events are alike (Durda et al., 2007); parent bodies experiencing a super-catastrophic disruption event may start with many more Bennu-sized fragments than one that merely had a barely-catastrophic or a cratering event. This could potentially allow either family to deliver more Bennu-sized asteroids than the other.

Estimating item (b) is non-trivial because both families have lost a substantial fraction of their starting SFDs to the J3:1 resonance (Figs. 7 and 8). To deal with this issue, and avoid a biased sample of objects, we have plotted in Fig. 20 the SFD of the left sides of the families (i.e., all known family members with

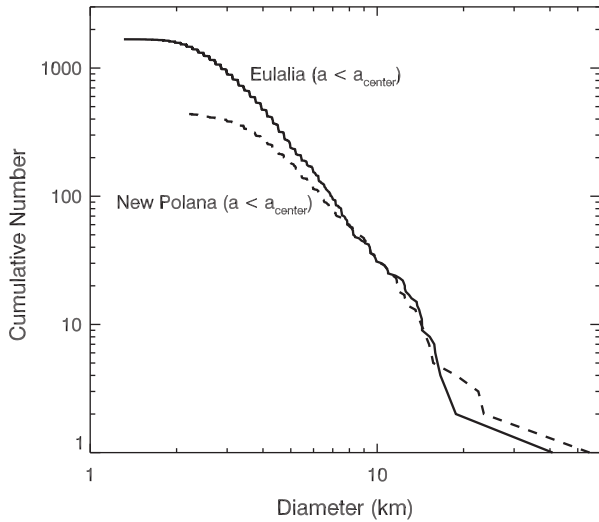


**Fig. 20.** A comparison of the size–frequency distributions for the Eulalia and New Polana families. They are drawn as solid and dashed lines, respectively, with the data taken from Figs. 6 and 7, respectively. To avoid complications with losses through the J3:1 resonance, we only examined the portions of each family with  $a < a_{\text{center}}$ . To convert from  $H$  to diameter, we assumed all asteroids had albedos  $p_v = 0.05$ . The size distributions are found to be similar for  $D > 8$  km. Below this point, the mismatches may be caused by a variety of sources (e.g., attrition from collisional evolution, loss of asteroids to the  $v_6$  resonance, observational selection effects, difficulty in identifying family members, etc.).

$a < a_{\text{center}}$ ). The largest members have yet to move far from the family center, and they are less complicated to interpret (i.e., the difficulty in identifying family members spread out in  $(a, e, i)$ , family members that could plausibly be part of either the Eulalia or New Polana families; depletion by collisional evolution; Fig. 8). Moreover, because both families have similar orbital and albedo parameters, we expect the selection effects associated with WISE observations to be about the same for each.

Here we find that the SFD of both families for  $D > 8$  km ( $H = 14.4$ ) are very similar to one another. The Eulalia SFD does become steadily larger for  $D < 8$  km, but this is also where a myriad of selection effects may start to play an increasingly important role. These large objects may also help keep the smaller objects resupplied by a collisional cascade. When modeling the collisional evolution of many kinds of asteroid families, Bottke et al. (2005c) found that the observed family members can often be used to predict the number of smaller members that exist below the detection limit. Accordingly, because we lack additional information at this time that could act as a tie-breaker, we will assume here that the ratio of starting Bennu-size objects in the Eulalia family over the New Polana family is  $r_{\text{pop}} = 1$ .

### 6.2.3. Collisional evolution within the Bennu source families

Item (c) involves how the two families react to roughly a billion years of collisional evolution within the main belt population. In a family, big objects disrupt infrequently, but they create fragments that replace, at some level, the population of smaller objects that disrupt more frequently. These sources and sinks are treated in an approximate manner in our model.

On the source side, breakup events among larger Eulalia and New Polana family members should be constantly replenishing the Bennu population (i.e., the collisional cascade). On the sink side of the ledger, the estimated mean collisional lifetime of Bennu-sized asteroids in the main belt ( $D = 0.5$  km) is several hundreds of Myr (Bottke et al., 2005a,b). Given that the estimated ages of Eulalia and New Polana are 0.8 and 1.4 Ga, respectively, only a fraction of the starting populations will make it to the  $v_6$  resonance

intact. In contrast, a  $D = 2$  km asteroid has a mean collisional lifetime of  $\sim 1$  Gyr, a value comparable to the ages of both families. This helps explain why the ears of these ancient families are still distinct.

To fully account for the above sources and sinks, we should ideally use a collisional and dynamical evolution model that can simultaneously account for how family members spread out with time while also undergoing a collisional cascade. This would allow us to account for breakup location; disruption near a resonance are more meaningful than those that take place near the family center. Unfortunately, no such model yet exists that can do this, though recent code developments may make this possible in the near future (Levison et al., 2012). The best we can do at present is estimate a collisional cascade “factor” using the 1-D collisional and dynamical depletion evolution model (CoDDEM) results of Bottke et al. (2005a,b,c).

CoDDEM is a self-consistent 1-D evolution code capable of tracking how multiple interacting small body populations can undergo comminution and dynamical depletion from the end of accretion to the present day. This model, when applied to the main belt, was able to reproduce all available main belt constraints germane to a 1-D code (e.g., the wavy shape of the main belt size distribution, the distribution of asteroid families produced by  $D > 100$  km parent bodies over the last 3.5 Gyr, etc.).

In Bottke et al. (2005c), CoDDEM was applied to the evolution of several generic asteroid families whose fragment SFD followed a power law. Using parent bodies with sizes between  $D = 123$  km and  $D = 195$  km, they tracked how collisional evolution modified the family SFD, including the population of Bennu-sized asteroids ( $D = 0.5$  km), over billions of years. Using these results, we calculated the number of Bennu-sized asteroids that were left in the families at 0.8 Gyr and at 1.4 Gyr. The ratio of surviving Bennu-sized bodies in Eulalia over New Polana is defined as  $r_{\text{coll}}$ . This value roughly accounts for item (c). Our results ranged between  $r_{\text{coll}} = 1.6$  and 1.7 for the  $D = 123$  and 195 km test families, respectively. To be conservative, we use  $r_{\text{coll}} = 1.6$  here.

### 6.2.4. Predicting the likely source of Bennu

Finally, for item (d), we have two components. We estimated above that the Eulalia and New Polana fluxes into the J7:2/M5:9 and  $v_6$  resonances is one-third and two-thirds of their net total. We call this fraction of the flux  $f_{\text{fract}}$ . We also need to include the results of the Bottke et al. (2002a) source predictor model, which favors the  $v_6$  resonance as a source of Bennu compared to the IMC region 82–18%. We call this factor  $f_{\text{NEO}}$ .

To put everything together and compare the families, we did the following. First, we converted the ratios above ( $r_{\text{flux}}, r_{\text{pop}}, r_{\text{coll}}$ ) into fractions of the net flux from each family entering either source region. Then, by source region, we multiplied these values by the appropriate weighting factors for those sources, namely  $f_{\text{fraction}}$  and  $f_{\text{NEO}}$ . We then added the components for each family together and took the ratio of the sums.

Our results yield the relative contribution from the Eulalia and New Polana families that can potentially make Bennu. They suggest that, on average, about twice as many New Polana objects are likely to reach Bennu’s orbit as Eulalia (2.4), with a spread between 1.9 and 3.7. From a probability standpoint, we found a  $70^{+8}_{-4}\%$  probability that Bennu came from New Polana and a  $30^{+8}_{-4}\%$  probability it came from Eulalia. Thus, the odds favor Bennu being from the New Polana family, though the Eulalia family is also a plausible source.

### 6.3. Checking the absolute flux of dark asteroids into the $v_6$ resonance

As a way of testing to see whether our absolute flux calculations for Eulalia and New Polana make sense, we compared our results to

the estimated flux rates of low albedo asteroids entering the  $\nu_6$  and IMC regions from Bottke et al. (2002a) and Morbidelli et al. (2002).

Morbidelli et al. (2002) determined that ratio of dark to bright asteroids in the entire NEO population as a function of diameter was 0.87. Converting this value, we find that 47% of the NEO population should be dark asteroids, where dark in their definition means an albedo  $p_v$  between 0.02 and 0.089, with a mean of 0.055. If we remove the dormant family comets in their defined population, this value is reduced to 33%, which is fairly similar to values estimated in Stuart and Binzel (2004), assuming their C-complex asteroids match the defined albedo range, and the debiased NEOWISE results from Mainzer et al. (2013). Only about 30–40% of these bodies have albedos consistent with Bennu, so the net fraction of interest is redefined to be 9–13%. To keep things simple, we will assume this value is 10%.

Bottke et al. (2002a) estimated that the absolute flux of  $H < 18$  asteroids exiting the  $\nu_6$  resonance per Myr was  $55 \pm 18$ , and that coming out of the IMC region was  $65 \pm 15$ . Using the Bottke et al. (2002a) size distribution for main belt asteroids, and the fact that an  $H = 18$  asteroid with an albedo  $p_v = 0.055$  becomes a  $D = 1.4$  km asteroid (see Fowler and Chillemi, 1992), we find there are about 5.5 times as many  $D = 0.5$  km asteroids as  $D = 1.4$  km asteroids. This means the flux of  $D > 0.5$  km asteroids entering the  $\nu_6$  resonance and IMC region per Myr is  $300 \pm 100$  and  $360 \pm 80$ , respectively. Multiplying this by the 10% value above, we find that  $30 \pm 10$  and  $36 \pm 8$  low albedo asteroids per Myr with  $D > 0.5$  km enter the  $\nu_6$  resonance and IMC region in the current era, respectively.

Using our flux values from Fig. 18, we find that the fraction of low albedo asteroids with  $D = 0.5$  km from the Eulalia or New Polana families entering the  $\nu_6$  resonance every 20 Myr is  $0.83_{-0.2}^{+0.03} \times 10^{-3}$  and  $2.1_{-0.3}^{+0.3} \times 10^{-3}$ . Combining values, we get a net fraction of 0.0029 every 20 Myr, or 0.00015 per Myr. Using the values in Walsh et al. (2013) and extrapolating from them, we estimate the number of  $D = 0.5$  km asteroids in the original Eulalia family was about  $1.5 \times 10^6$ , give or take a factor of 2. Note that the New Polana contribution was similar (i.e.,  $f_{\text{pop}} = 1$ ), such that its contribution was included when the fluxes above were added together. Collisional evolution estimates from Bottke et al. (2005c) indicate this initial population should be reduced by about a factor of 10 between 0.8 and 1.4 Gyr, yielding  $1.5 \times 10^5$  bodies with  $D > 0.5$  km today. Multiplying this value by the fraction entering the  $\nu_6$  resonance of 0.00015 per Myr, we get  $22_{-4}^{+3}$  low albedo  $D > 0.5$  km asteroids per Myr entering the  $\nu_6$  resonance. We consider this to be a reasonable match to the estimated flux above of  $30 \pm 10$ .

For the IMC region, we find that the fraction of low albedo asteroids with  $D = 0.5$  km from the Eulalia or New Polana families entering the  $\nu_6$  resonance every 20 Myr is  $1.1_{-0.6}^{+0.3} \times 10^{-3}$  and  $1.1_{-0.2}^{+0.2} \times 10^{-3}$ , respectively. Combined, this yields a net fraction of 0.0022 every 20 Myr, or 0.00011 per Myr. Multiplying this value by  $1.5 \times 10^5$  bodies, we get  $17_{-6}^{+3}$  low albedo  $D > 0.5$  km asteroids per Myr entering the IMC region. This value is about half of the estimated flux from above of  $36 \pm 8$ .

Given our uncertainties, we believe that obtaining values within a factor of two of the estimated fluxes is a surprising success. They provide a valuable consistency check on our work, and give us increased confidence that we are on the right track. With that said, if these differences are meaningful, and they are not caused by inaccurate approximations or modeling results, we can perhaps say a few things about the mismatch for the IMC region.

First of all, the flux rates from Bottke et al. (2002a) and Morbidelli et al. (2002) are for all possible inclinations, while our Eulalia and New Polana results are only for low inclinations ( $i < 6^\circ$ ). Thus, the fact that our family flux rates for the  $\nu_6$  resonance are comparable to predictions means most small low albedo

asteroids must come from Eulalia and New Polana families. For the IMC region, we know it is replenished by many additional resonances further out in the inner main belt, as well as by high eccentricity objects drifting by the Yarkovsky effect into the Mars-crossing region. Bottke et al. (2002a) even found objects from the J3:1 can be mixed into the IMC region. The fact that our family flux rates are about half that predicted means these additional ways to replenish the IMC region may be important. Some could also be providing higher inclination bodies than Eulalia and New Polana family members. Thus, while they would be unlikely to produce Bennu (e.g., Fig. 2), they could still account for the missing flux.

Second, Fig. 19 shows that flux of New Polana and, to a lesser degree, Eulalia family members into the J7:2/M5:9 resonance was much larger in the past. If we were to include the effects of a collisional cascade, with larger slower inward-drifting asteroids disrupting and replenishing Bennu-sized bodies over time, it would probably shift the flux peak to older ages. This could readily lead to a higher present-day flux. Interestingly, this effect would have a smaller impact on the flux reaching the  $\nu_6$  resonance, such that this explanation would be very consistent with predictions.

Overall, our work implies that Eulalia and New Polana together dominate the population of low albedo Bennu-like asteroids coming from the  $\nu_6$  resonance and IMC region. If not, we would expect to see order of magnitude differences between our model flux and the predicted flux. Instead, our apparent match allows us to make some interesting calculations.

For example, Bottke et al. (2002a) estimate that the innermost region of the main belt (i.e., the  $\nu_6$  resonance and IMC region) produces about 80% of our Atens. This implies that most of the very dark  $D = 0.5$  km asteroids found there are probably from the Eulalia and New Polana families, with the former favored over the latter. Similar trends should be found among the asteroids with very Earth-like orbits (i.e.,  $a \sim 1$  AU, low  $e, i$  values), which are prime targets for exploration by robotic and human spacecraft. This raises the likelihood that missions to such low albedo NEOs may end up exploring fragments from the same two main belt families. On the other hand, for bodies in these populations that are considerably smaller than Bennu, the flux from families like Erigone should start to play an increasingly important role.

## 7. Discussion

### 7.1. Exploring the source families of other dark asteroid mission targets

Several other low albedo NEOs have been suggested as possible targets for upcoming sample return missions. The target of the upcoming Hayabusa 2 mission is the low albedo asteroid (162173) 1999 JU3. ESA's Marco Polo-R mission originally selected dark asteroid (175706) 1996 FG3 as its preliminary baseline target. Recently, however, the team switched to (341843) 2008 EV5 because of its favorable orbital characteristics, which offer the possibility of completing the entire mission in 4.5 years. 2008 EV5 also offers a moderate albedo and spectral properties that make it even more interesting for sample science. The rationale behind these missions is the same as that of OSIRIS-REX, namely they provide the opportunity to investigate and return to the Earth uncontaminated primitive material.

It is interesting to compare and contrast these NEOs with Bennu using our model results. To keep things simple, we will refer to all of these asteroids by the letters and numbers of their last name.

(162173) 1999 JU3. JU3 is a Cg-class body larger than Bennu in terms of albedo and diameter (Binzel et al., 2001; Campins et al., 2013). The Cg class is also different from B-class Bennu. Spitzer observations by Campins et al. (2009) provided a geometric albedo of  $p_v = 0.07 \pm 0.01$  and a diameter of  $0.90 \pm 0.14$  km. Using three

sets of published thermal observations (ground-based N-band, Akari IRC, and Spitzer IRS), Mueller et al. (2011) derived an effective diameter of  $0.87 \pm 0.03$  km. The albedo was  $p_v = 0.070 \pm 0.006$ . They also suggest JU3 has a retrograde spin vector like Bennu. Similar results were found by Hasegawa et al. (2008), who used the AKARI space telescope and ground based measurements from Subaru to estimate an albedo of 0.063 and a diameter of  $D = 0.92 \pm 0.12$  km. The  $(a, e, i)$  parameters of JU3, namely (1.19 AU, 0.19,  $5.9^\circ$ ), suggest it has an 80% and 20% probability of coming from the  $\nu_6$  resonance and IMC regions, respectively, by the Bottke et al. (2002a) model.

**(175706) 1996 FG3.** Walsh et al. (2012b) finds that FG3 is a binary B-type asteroid with a geometric albedo  $p_v = 0.039 \pm 0.012$  and a primary diameter of  $D = 1.9 \pm 0.28$  km. Its orbital parameters  $(a, e, i)$  of (1.05 AU, 0.35,  $2.0^\circ$ ) yield a 92% and 8% probability that it came from the  $\nu_6$  resonance and IMC region, respectively, according to the Bottke et al. (2002a) model. It has a retrograde spin vector as well.

**(341843) 2008 EV5.** EV5 is a C-type asteroid (Somers et al., 2008; Reddy et al., 2012; Alí-Lagoa et al., 2014) that has been observed by radar by Busch et al. (2011). They find that its diameter is  $D = 0.4 \pm 0.05$  km. Like Bennu, it has a roughly top-like shape with an equatorial ridge. Busch et al. (2011) also report an albedo of  $p_v = 0.12 \pm 0.04$ , a value that has been verified by Reddy et al. (2012). This value is much higher than for the others asteroids discussed here. The  $(a, e, i)$  parameters of EV5, namely (0.96 AU, 0.08,  $7.4^\circ$ ), suggest it has an 51% and 49% probability of coming from the  $\nu_6$  resonance and IMC regions, respectively, according to the Bottke et al. (2002a) model.

The JU3 and FG3 asteroids, both with relatively low albedos and high probabilities of coming from the  $\nu_6$  resonance, can be investigated with the model presented here. Tests using the procedure in Section 3 indicate both appear to come from the same range of main belt starting inclinations as Bennu, and all have retrograde spin vectors, implying they evolved inward by the Yarkovsky effect until they reached the  $\nu_6$  resonance or the IMC region.

With this said, the taxonomy of JU3 is Cg-class, and its albedo is 0.07, both which are different from Bennu. Thus, it is possible our low albedo low inclination families in the inner main belt could be ruled out as sources on this basis (see Campins et al., 2013). We caution, however, that spectra from C-complex bodies are defined by slope rather than spectral bands, and therefore are less diagnostic of family membership (Binzel, personal communication). Additional work is needed to fully characterize the spread in spectral signatures within the families discussed here, as well as their fragments' spectra changes with distance from the Sun, temperature, size, orbital history, etc. Masiero et al. (2011, 2013) also show that families often have a modest spread in albedo values around their mean values. For these reasons, we believe it is reasonable to apply our model to both JU3 and FG3, with the caveats above noted.

On the other hand, our model probably should not be applied to EV5 without modifications. EV5 has a high albedo for a C-complex asteroid (0.12), which means it may not come from the families discussed here. In addition, C/X-complex inner main belt families with mean albedos  $>0.1$ , such as possibly the Baptistina family (Parker et al., 2008; Delbò and Michel, 2011; Masiero et al., 2013; see also Bottke et al., 2007 and Masiero et al., 2011 for background material) would potentially need to be considered as source families. We have also yet to explore the characteristics of background inner main belt asteroids with these kinds of albedos. A complete workup of EV5 will be reserved for another time.

Using the logic applied above for Bennu, we can quickly rule out the Clarissa, Erigone, and Sulamitis families as a possible source for JU3 and FG3. If these families cannot produce a  $D = 0.5$  km NEO with an Bennu-like orbit, things are even worse for larger asteroids

with slower Yarkovsky drift rates. This once again leaves Eulalia and New Polana families as the most plausible sources.

**(162173) 1999 JU3.** In Fig. 21, where  $\tau_{\text{YORP}}$  value was set to 0.25 Myr, we show the influx rate for the Eulalia and New Polana families for JU3-sized asteroids ( $D = 0.87$  km). It shows the fraction of the starting population from the Eulalia family reaching the  $\nu_6$  and J7:2/M5:9 resonances per 20 Myr in the current era is  $0.8^{+0.1}_{-0.05} \times 10^{-3}$  and  $1.5^{+0.3}_{-0.7} \times 10^{-3}$ , respectively. For the New Polana family, the values are  $2.3^{+0.2}_{-0.3} \times 10^{-3}$  and  $1.8^{+0.4}_{-0.4} \times 10^{-3}$ , respectively. The ratio of the fluxes from Eulalia to New Polana entering the  $\nu_6$  and IMC regions  $r_{\text{flux}}$  are  $0.34^{+0.09}_{-0.05}$  and  $0.88^{+0.45}_{-0.49}$ , respectively. The value of  $f_{\text{coll}}$  for JU3-sized bodies is close to that of Bennu, namely 1.5–1.6.

Putting the factors together as with Bennu, we find that on average, 2.7 times as many JU3-sized bodies from the New Polana family reach a JU3-type orbit, with a spread between 2.1 and 3.3. Thus, JU3 has a  $73^{+5}_{-4}\%$  probability of coming from the New Polana family and a  $27^{+4}_{-5}\%$  probability of coming from the Eulalia family. These values are similar to those of Bennu, not surprising given the similar orbits and sizes of both bodies (0.5 km for Bennu vs. 0.87 km for JU3).

**(175706) 1996 FG3.** Our results for FG3 are even more interesting. The influx rate from the Eulalia and New Polana families for FG3 are shown in Fig. 22, where we assumed FG3 was  $D = 1.9$  km. The  $\tau_{\text{YORP}}$  value for these larger objects was set to 0.5 Myr. Here see several spikes for Eulalia and New Polana as their ears enter the  $\nu_6$  and J7:2/M5:9 resonances. In fact, they suggest Eulalia may be producing a spike of low albedo 1.9 km objects today via the  $\nu_6$  resonance. Overall, the fraction of the starting population from the Eulalia family reaching the  $\nu_6$  and J7:2/M5:9 resonances per 20 Myr in the current era are  $11^{+2}_{-11} \times 10^{-3}$  and  $1.7^{+0.5}_{-1} \times 10^{-3}$ , respectively. For the New Polana family, the values are  $1.9^{+0.4}_{-0.3} \times 10^{-3}$  and  $0.8^{+0.3}_{-0.2} \times 10^{-3}$ , respectively. The ratio of the fluxes from Eulalia to New Polana entering the  $\nu_6$  and IMC regions  $r_{\text{flux}}$  are  $5.8^{+2.3}_{-5.8}$  and  $2.1^{+1.5}_{-1.5}$ , respectively.

In this case, we find that Eulalia beats New Polana, with 5.5 times as many FG3-sized bodies reaching an FG3-type orbit. The potential spread is enormous, 0–7.8, because the age of the family essentially covers the flux spike seen in Fig. 22 for the  $\nu_6$  resonance. Putting these values together, we find FG3 has a  $85^{+4}_{-83}\%$  probability

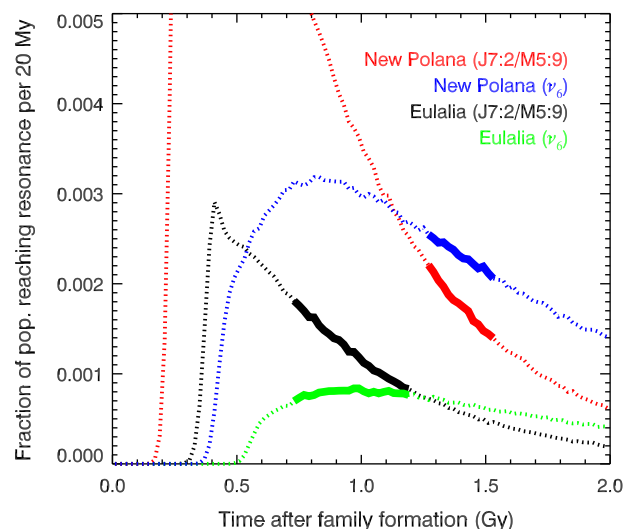


**Fig. 21.** The estimated flux of JU3-sized bodies ( $D = 0.87$  km) entering the  $\nu_6$  resonance and IMC regions over time from the Eulalia and New Polana families. See Fig. 19 for details. The  $\tau_{\text{YORP}}$  value here was set to 0.25 Myr.

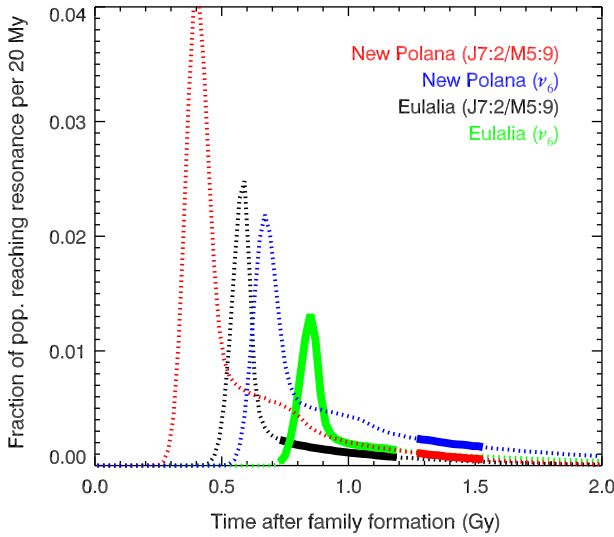


**Fig. 22.** The estimated flux of FG3-sized bodies ( $D = 1.9$  km) entering the  $\nu_6$  resonance and IMC regions over time from the Eulalia and New Polana families. See Fig. 19 for details. The  $\tau_{\text{YORP}}$  value here was set to 0.5 Myr.

of coming from the Eulalia family and a  $15^{+83}_{-4}\%$  probability of coming from the New Polana family.

Using the methods discussed in Section 6.3, it is instructive to compare our estimated fluxes to those predicted from Bottke et al. (2002a) and Morbidelli et al. (2002). In Section 6.3, we estimated that 10% of the  $55 \pm 18$  asteroids with  $H < 18$  and albedo  $0.02 < p_v < 0.055$  enter the  $\nu_6$  resonance every Myr. FG3 is  $D \sim 1.9$  km, and an  $H = 18$  is 1.66 km for  $p_v = 0.04$ . Using a main belt size distribution, we estimate that the flux is 1.2 times smaller for  $D = 1.9$  km bodies than 1.66 km bodies. This yields a net flux of  $4.6 \pm 1.5$  FG3-sized bodies entering the  $\nu_6$  resonance per Myr. The estimated fraction of Eulalia and New Polana bodies entering the  $\nu_6$  resonance for FG3-sizes is  $13^{+2.4}_{-11} \times 10^{-3}$  per 20 Myr, or  $0.65^{+0.12}_{-0.55} \times 10^{-3}$ .

A rough estimate of the number of FG3-sized bodies for Eulalia and New Polana can be obtained from Fig. 20 by extrapolating the slope of the Eulalia size distribution for  $3 < D < 7$  km bodies to 1.9 km bodies. We choose Eulalia here because the New Polana family is poorly characterized at small sizes. Our estimate yields about 4500 bodies. The value of  $f_{\text{coll}}$  for FG3-sized bodies is  $\sim 1.2$ . Put together, we get  $2.4^{+0.5}_{-2}$ . These results are similar within the errors, remarkable given our uncertainties. We infer that these two families produce most low albedo FG3-sized NEOs coming out of the  $\nu_6$  resonance, and therefore they also produce most of the FG3-like bodies seen among the Aten and Earth-like orbit populations.

We conclude from these calculations that there is a transition that takes place between 1 and 2 km for these two families in terms of asteroids on Earth-like orbits likely to be visited by spacecraft. The New Polana family appears to produce most of the low albedo  $D < 1$  km NEOs on Earth-like orbits, while Eulalia delivers most of the low albedo  $D > 1$  km asteroids. The reason for the switch is a function of the family’s age, the family’s proximity to the  $\nu_6$  and J7:2/M5:9 resonances, YORP cycles, and how long the ear persists in different families for difference sizes.

## 7.2. The implications of stochastic YORP for asteroid shapes

Small asteroids appear to come in all shapes and sizes. Some have top-like shapes like Bennu (e.g., 1994 KW4), while others

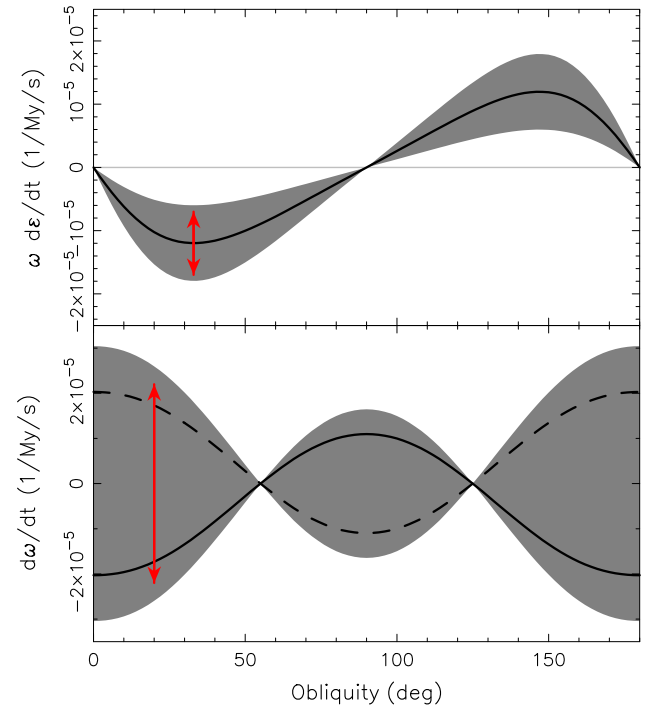


**Fig. 23.** Dependence of the  $f$ - and  $g$ -functions from Eqs. (2) and (3) on the obliquity  $\epsilon$ : (i)  $g = \omega(d\epsilon/dt)$  at the top panel ( $\omega$  is the rotation rate), and (ii)  $f = d\omega/dt$  at the bottom panel. The ordinate scale is for a  $D = 2$  km body at  $a = 2.5$  AU heliocentric distance and a bulk density of  $\rho_{\text{bulk}} = 2.5$  g/cm<sup>3</sup>. The appropriate scaling to other parameter values is given by  $\propto 1/(\rho_{\text{bulk}} a^2 D^2)$ . The solid lines are “nominal values”, determined and averaged over a sample of 200 Gaussian spheres by Čapek and Vokrouhlický (2004); we used their highest conductivity run appropriate for small asteroids. In the case of the rotation rate, the averages were done separately for asymptotically accelerating and decelerating bodies (dashed and solid lines). The grey zone indicates the variance of the results.

are highly elongated and look like a few large blocks held together by gravity alone (e.g., Itokawa; Toutatis). This diversity has yet to be fully characterized, but asteroid shapes derived from radar observations and lightcurve inversion techniques indicate many configurations are possible.

This apparent variety, however, had long been a curiosity to those of us who believed the static YORP effect dominated the spin rate evolution of small asteroids. According to this model, the majority of small asteroids reside in the main belt long enough to experience multiple YORP cycles. This would make it almost inevitable that the majority would ultimately spin up fast enough to shed mass. Too many of these incidents would cause small asteroids to eject their most fragile components. Over time, one could envision the creation of a small asteroid shape distribution dominated by tops or single blocks, which is not observed.

The advent of stochastic YORP, however, may help explain this puzzle. If all small asteroids undergo a random walk in spin rate, some fraction may stay far from any meaningful YORP endstates throughout their lifetime. This could allow them to keep the structural traits produced when they were created in a family-forming event. Others may undergo numerous mass shedding events, perhaps far more than a typical asteroid of the same size. This mass-shedding “buzzsaw” might eventually whittle them into a top-like shape over a much faster timescale than expectations from a static YORP model.

Modeling the effects of stochastic YORP on asteroid shapes is beyond the scope of this paper, but we believe it could be an interesting project for the future.

## 8. Conclusions

In this paper, we investigated the probable source of Bennu using a suite of numerical models. We summarize our major results below.

(a) The known characteristics of Bennu indicate it (and/or its modestly larger precursor) evolved inward across the main belt from a low albedo family by the Yarkovsky effect over many hundreds of Myr. It eventually entered a source region for NEOs, where it traveled to its current orbit in probably a few Myr to tens of Myr (Section 2).

(b) We have tracked the evolution of thousands of model asteroids started near the most likely main belt source regions for Bennu, namely the  $\nu_6$  secular resonance, the intermediate source Mars-crossing region (IMC region), and the J3:1 mean motion resonance with Jupiter (J3:1). We have found that the best source region to produce Bennu is the  $\nu_6$  resonance. A less likely source is the IMC region. The J3:1 is very unlikely to produce Bennu. Using results from Bottke et al. (2002a), we predict the relative probabilities of Bennu coming from the  $\nu_6$  resonance and the IMC region is 82–18%, respectively (see also Campins et al., 2010) (Section 3).

(c) The asteroid orbital parameters in the NEO source region most likely to produce Bennu have oscillating eccentricities between  $0.1 < e < 0.2$  and inclinations between  $1^\circ < i < 6^\circ$ , with a preference for  $3^\circ < i < 4^\circ$ . This implies the low albedo families that produced Bennu had similar orbital characteristics (Section 3).

(d) Five families have the appropriate dynamical, spectral, and albedo characteristics to potentially produce Bennu: Erigone, Sulamitis, Clarissa, Eulalia, and New Polana (Section 4).

(e) We created a Yarkovsky–YORP model that reproduced the spin rate and obliquity constraints from small asteroids. This model assumes no changes are made between YORP endstates, namely spinning-up so fast that the asteroid sheds mass or spinning so slowly that the asteroid enters into a tumbling rotation state. We call this a “static YORP” model. The interval needed to go from starting conditions to endstate is defined as a “YORP cycle”. The static YORP model has been used successfully to reproduce the  $(a, H)$  distributions of young asteroid families like Erigone (Vokrouhlický et al., 2006a,b) (Section 5).

(f) The calibrated static YORP model suggests there is a preference for spinning down vs. spinning up for small asteroids, with our best fit  $\delta_{\text{YORP}} \simeq 0.4$ . For reference, a 50–50 split would come from a value of 0.5. Our best fit value of  $c_{\text{YORP}} \simeq 0.5 - 0.7$  (nominal is 1) also suggests YORP is somewhat weaker than expected. This supports the modeling results of Rozitis and Green (2012) (Section 5).

(g) Our static YORP model cannot reproduce the observed  $(a, H)$  configuration of older families like Eulalia and New Polana. The reason is that small asteroids undergo numerous YORP cycles, which cause their obliquities to flip from time to time. These changes produce a random walk in semimajor axis, with the changing Yarkovsky drift  $da/dt$  direction preventing the asteroids from moving anywhere quickly. This work implies the static YORP model must be corrected to accurately treat Bennu-sized bodies coming from older families like Eulalia and New Polana (Section 5).

(h) Our solution was to implement into our code the “stochastic YORP” concept from Statler (2009) (see also Cotto-Figueroa, 2013, submitted for publication). Statler (2009) showed that small asteroids undergo small but meaningful shape changes via a variety of physical processes between their YORP endstates (e.g., cratering events, downslope movement, reaction of the asteroid’s shape to changes in the rotational angular momentum budget via YORP, etc.), and that these modifications cause the spin rate, but not the obliquity, to undergo a random walk. This prevents many

bodies from reaching YORP endstates as quickly as in the static YORP case. The lower frequency of YORP cycles allows asteroids like Bennu to travel further in a given semimajor axis direction than before. To reproduce the observed  $(a, H)$  distribution of Eulalia, we assumed that the timescale for meaningful shape changes occurs  $>10$  times more frequently than the YORP cycle timescale for a given asteroid size (Section 5).

(i) Using the stochastic YORP model, and making certain assumptions about the physical parameters of our model family members, we estimate the ages of the Clarissa, Erigone, Eulalia, New Polana, and Sulamitis families to be  $\sim 60$  Myr old,  $130 \pm 30$  Myr old,  $830^{+370}_{-100}$  Myr old, and  $1400 \pm 150$  Myr old, and  $200 \pm 40$  Myr, respectively. Our results also show Bennu-sized asteroids from Eulalia and New Polana, but not Erigone, Clarissa, and Sulamitis, can reach the  $\nu_6$  and J7:2/M5:9 resonances, with the latter feeding the IMC source region, within the age of the family (Section 6).

(j) The results of our stochastic YORP model, which includes a wide range of factors (e.g., the flux of Bennu-like bodies into NEO source regions like the  $\nu_6$  resonance and the IMC region, the parent body/family size, collisional evolution, etc.) indicate that, on average, about twice as many New Polana objects are likely to reach Bennu’s orbit as those from Eulalia. Formally, this ratio is 2.4 with range between 1.9 and 3.6. This corresponds to the New Polana and Eulalia families having a  $70^{+4}_{-2}\%$  and  $30^{+4}_{-8}\%$  probability of producing Bennu, respectively (Section 6).

(k) Our estimates of the net flux of low albedo Bennu-sized asteroids entering the  $\nu_6$  resonance are consistent with complementary calculations derived from the numerical results of Bottke et al. (2002a) and Morbidelli et al. (2002). They suggest the Eulalia and New Polana families completely dominate the flux of dark  $D = 0.5$  km asteroids entering the  $\nu_6$  resonance, with a net flux rate of  $24^{+4}_{-7}$  Bennu-sized objects entering the resonance per Myr. The predicted value was  $30 \pm 10$  per Myr. These same families produce less than half of the estimated flux of similar bodies entering the IMC region ( $14^{+2}_{-3}$  vs.  $36 \pm 8$  per Myr). We believe the remainder may come from alternative, higher inclination sources not modeled here. Trends in our results also suggest a possible fix could come from explicitly including a collisional cascade within our model (Section 6).

(l) We also investigated the likely source families of two low albedo asteroids that may be sample return candidates: the  $D = 0.87$  km asteroid (162173) 1999 JU3 and the  $D = 1.9$  km asteroid (175706) 1996 FG3. Both have Earth-like orbits fairly similar to that of Bennu, and are favored to come from the  $\nu_6$  resonance and IMC regions. We find that  $\sim 2.7$  times as many JU3-sized bodies from the New Polana family reach a JU3-type orbit as Eulalia. This means that JU3 has a  $73^{+5}_{-4}\%$  probability of coming from the New Polana family and a  $27^{+4}_{-5}\%$  probability of coming from the Eulalia family. These values are similar to those of Bennu. Perhaps surprisingly, Eulalia beats New Polana for FG3-sized objects, with 5.5 times as many FG3-sized bodies reaching an FG3-type orbit. We find FG3 has a  $85^{+4}_{-83}\%$  probability of coming from the Eulalia family and a  $15^{+83}_{-4}\%$  probability of coming from the New Polana family. The factors responsible for this turnabout include each family’s age, their proximity to the  $\nu_6$  and J7:2/M5:9 resonances, YORP cycles, and how long a family’s “ear” persists in for different asteroid sizes.

(m) We speculate that our stochastic YORP model explains why some asteroids have managed to maintain their somewhat fragile shapes against YORP spin-up, with a random walk in spin rate keeping some bodies away from overly-fast spin rates. Others may enter into a fast-spin mass-shedding state numerous times, with a possible consequence being a top-like shape with an equatorial band as seen for Bennu (Section 7).

These predictions are the best we can do with the information we have at this time. We are certain, however, that as we learn more about Bennu, its samples, and its potential source families Eulalia and New Polana, we will be able to do better. In fact, it is our expectation that some telltale clues provided by the OSIRIS-REx mission, possibly found within the samples themselves, will allow us to choose between the possibilities presented here.

## Acknowledgements

We thank Valerio Carruba and an anonymous referee for their careful and constructive reviews that improved this paper. We also thank the innumerable helpful comments and suggestions that came from members of the OSIRIS-REx science team. Research funds for William Bottke were provided by NASA's OSIRIS-REx mission; NASA Contract NNM10AA11C (D.S. Lauretta, PI). Support for Kevin Walsh came from the Center for Lunar Origin and Evolution of NASA's Lunar Science Institute, and NASA's Solar System Evolution Research Virtual Institute (SSERVI) program through a grant to the Institute for the Science of Exploration Targets (NNA14AB03A), at the Southwest Research Institute in Boulder. The work of David Vokrouhlický was partially supported by research grant P209-13-01308S of the Czech Grant Agency. Marco Delbo and Patrick Michel acknowledge support from the French CNES. Resources supporting this work were provided by the NASA High-End Computing (HEC) Program through the NASA Advanced Supercomputing (NAS) Division at Ames Research Center.

## Appendix A. Further discussion of the effects of stochastic YORP

Here we provide additional discussion of how stochastic YORP affects an asteroid's rotation rate and obliquity. Čapek and Vokrouhlický (2004) calculated the strength of YORP for 200 synthetic asteroid shapes (i.e., Gaussian spheres, basically potato-like bodies). For each test asteroid, they determined  $g$ - and  $f$ -functions from the following YORP representation valid when the body rotates about the shortest principal axis of the inertia tensor:

$$\frac{d\omega}{dt} = f(\epsilon), \quad (2)$$

$$\frac{d\epsilon}{dt} = \frac{g(\epsilon)}{\omega}. \quad (3)$$

Here  $\omega$  is the rotation rate and  $\epsilon$  is the obliquity. Both  $f$  and  $g$  are functions of the obliquity  $\epsilon$  (see Fig. 23). The function  $f$  does not depend on the surface thermal inertia, while  $g$  generally decreases as the surface thermal inertia increases. Both are symmetric or anti-symmetric about the  $\pi/2$  obliquity state. The behavior of the  $g$ -function is anti-symmetric when  $\epsilon \rightarrow \pi - \epsilon$  and negative when  $\epsilon < \pi/2$ . The  $f$ -function is symmetric when  $\epsilon \rightarrow \pi - \epsilon$  and generally has a zero point near obliquities of  $55^\circ$  or  $135^\circ$  (nodes of the second degree Legendre polynomial; see Nesvorný and Vokrouhlický, 2007; Breiter and Michałska, 2008). The  $f$  values at 0 or  $\pi$  obliquity may be positive or negative, indicating the body may asymptotically accelerate or decelerate its rotation rate  $\omega$ . As a result, the solid and dashed lines at the bottom panel of Fig. 23 show the median  $f$  behavior in the respective range of asymptotic acceleration or deceleration, while the variance zone of all possible  $f$ -function behavior is shown by the gray zone.

In our static YORP model, we choose, for a given body, one possible pair of  $f$ - and  $g$ -functions from the gray regions in Fig. 23 and keep them until the rotation state evolves toward the asymptotic situation. Then, the initial rotation state is selected anew and new  $f$ - and  $g$ -functions are chosen.

Conversely, in the stochastic YORP model, we choose new  $f$ - and  $g$ -functions once a given time  $\tau_{\text{YORP}}$  has elapsed. This does not

fundamentally change how the obliquity evolves, but it does modify the rate of the obliquity change. Regardless, the important feature is that the obliquity again converges toward the known asymptotic states. The main modification in the code concerns the rotation rate evolution:  $\omega$  now evolves towards an asymptotic state through a random-walk process (by having random-sign contributions at different intervals of time) rather than continuous flow. This arrangement extends the duration of the YORP cycle while maintaining bodies at extreme obliquity values. This helps to move them efficiently by the Yarkovsky forces in semimajor axis.

## References

- Alfí-Lagoa, V., Lionni, L., Delbo, M., Gundlach, B., Blum, J., Licandro, J., 2014. Thermophysical properties of near-Earth asteroid (341843) 2008 EV<sub>5</sub> from WISE data. *Astron. Astrophys.* 561, A45.
- Benavidez, P.G., Durda, D.D., Enke, B.L., Bottke, W.F., Nesvorný, D., Richardson, D.C., Asphaug, E., Merline, W.J., 2012. A comparison between rubble-pile and monolithic targets in impact simulations: Application to asteroid satellites and family size distributions. *Icarus* 219, 57–76.
- Binzel, R.P., Harris, A.W., Bus, S.J., Burbine, T.H., 2001. Spectral properties of near-Earth objects: Palomar and IRTF results for 48 objects including spacecraft targets (9969) Braille and (10302) 1989 ML. *Icarus* 151, 139–149.
- Bottke, W.F., Asphaug, E., 2013. On the origin and evolution of differentiated planetesimals. *Lunar Planet. Inst. Sci. Conf. Abstr.* 44, 1672.
- Bottke, W.F., Melosh, H.J., 1996. Binary asteroids and the formation of doublet craters. *Icarus* 124, 372–391.
- Bottke, W.F., Rubincam, D.P., Burns, J.A., 2000. Dynamical evolution of main belt meteoroids: Numerical simulations incorporating planetary perturbations and Yarkovsky thermal forces. *Icarus* 145, 301–331.
- Bottke, W.F., Brož, M., Nesvorný, D., Morbidelli, A., 2001. Dynamical spreading of asteroid families via the Yarkovsky effect. *Science* 294, 1693–1696.
- Bottke, W.F., Morbidelli, A., Jedicke, R., Petit, J.-M., Levison, H.F., Michel, P., Metcalfe, T.S., 2002a. Debaised orbital and absolute magnitude distribution of the near-Earth objects. *Icarus* 156, 399–433.
- Bottke, W.F., Vokrouhlický, D., Rubincam, D.P., Brož, M., 2002b. Dynamical evolution of asteroids and meteoroids using the Yarkovsky effect. In: Bottke, W.F. et al. (Eds.), *Asteroids III*. University of Arizona Press, Tucson, pp. 395–408.
- Bottke, W.F., Durda, D.D., Nesvorný, D., Jedicke, R., Morbidelli, A., Vokrouhlický, D., Levison, H.F., 2005a. The fossilized size distribution of the main asteroid belt. *Icarus* 175, 111–140.
- Bottke, W.F., Durda, D.D., Nesvorný, D., Jedicke, R., Morbidelli, A., Vokrouhlický, D., Levison, H.F., 2005b. Linking the collisional history of the main asteroid belt to its dynamical excitation and depletion. *Icarus* 179, 63–94.
- Bottke, W.F. et al., 2005c. The origin and evolution of stony meteorites. In: Knežević, Z., Milani, A. (Eds.), *Dynamics of Populations of Planetary Systems*. Cambridge University Press, Cambridge, pp. 357–374.
- Bottke, W.F., Vokrouhlický, D., Rubincam, D.P., Nesvorný, D., 2006a. The Yarkovsky and YORP effects: Implications for asteroid dynamics. *Ann. Rev. Earth Planet. Sci.* 34, 157–191.
- Bottke, W.F., Nesvorný, D., Grimm, R.E., Morbidelli, A., O'Brien, D.P., 2006b. Iron meteorites as remnants of planetesimals formed in the terrestrial planet region. *Nature* 439, 821–824.
- Bottke, W.F., Vokrouhlický, D., Nesvorný, D., 2007. An asteroid breakup 160 My ago as a probable source of the K-T impactor. *Nature* 449, 48–53.
- Bowell, E., Muinonen, K., Wasserman, L.H., 1994. A public-domain asteroid orbit database. In: Milani, A. et al. (Eds.), *Asteroids, Comets, Meteors 1993*. Kluwer, Dordrecht, pp. 477–481.
- Breiter, S., Michałska, H., 2008. YORP torque as the function of shape harmonics. *Mon. Not. Roy. Astron. Soc.* 388, 927–944.
- Breiter, S., Bartač, P., Czekaj, M., Oczujda, B., Vokrouhlický, D., 2009. The YORP effect on 25143 Itokawa. *Astron. Astrophys.* 507, 1073–1081.
- Breiter, S., Vokrouhlický, D., Nesvorný, D., 2010. Analytical YORP torques model with an improved temperature distribution function. *Mon. Not. Roy. Astron. Soc.* 401, 1933–1949.
- Britt, D.T., Yeomans, D., Housen, K., Consolmagno, G., 2002. Asteroid Density, Porosity, and Structure. In: *Asteroids III*, pp. 485–500.
- Brož, M., Morbidelli, A., Bottke, W.F., Rozehnal, J., Vokrouhlický, D., Nesvorný, D., 2013. Constraining the cometary flux through the asteroid belt during the late heavy bombardment. *Astron. Astrophys.* 551, A117 (16pp).
- Busch, M.W., 12 colleagues, 2011. Radar observations and the shape of near-Earth asteroid 2008 EV<sub>5</sub>. *Icarus* 212, 649–660.
- Burbine, T.H., McCoy, T.J., Meibom, A., Gladman, B., Keil, K., 2002. Meteoritic parent bodies: Their number and identification. In: Bottke, W.F., Cellino, A., Paolicchi, P., Binzel, R.P. (Eds.), *Asteroids III*. University of Arizona Press, pp. 653–667.
- Campins, H., Emery, J.P., Kelley, M., Fernández, Y., Licandro, J., Delbó, M., Barucci, A., Dotto, E., 2009. Spitzer observations of spacecraft target 162173 (1999 JU<sub>3</sub>). *Astron. Astrophys.* 503, L17–L20.
- Campins, H., Morbidelli, A., Tsiganis, K., de León, J., Licandro, J., Lauretta, D., 2010. The origin of asteroid 101955 (1999 RQ36). *Astrophys. J.* 721, L53–L57.
- Campins, H. et al., 2013. The origin of Asteroid 162173 (1999 JU<sub>3</sub>). *Astron. J.* 146, 26.

- Čapek, D., Vokrouhlický, D., 2004. The YORP effect with finite thermal conductivity. *Icarus* 172, 526–536.
- Carruba, V., 2010. Dynamical erosion of asteroid groups in the region of the Phocaea family. *Mon. Not. R. Astron. Soc.* 403, 1834–1848.
- Carruba, V., Burns, J.A., Bottke, W., Nesvorný, D., 2003. Orbital evolution of the Gefion and Adeona asteroid families: Close encounters with massive asteroids and the Yarkovsky effect. *Icarus* 162, 308–327.
- Carruba, V., Michtchenko, T.A., Roig, F., Ferraz-Mello, S., Nesvorný, D., 2005. On the V-type asteroids outside the Vesta family. I. Interplay of nonlinear secular resonances and the Yarkovsky effect: The cases of 956 Elisa and 809 Lunda. *Astron. Astrophys.* 441, 819–829.
- Carruba, V., Huaman, M., Domingos, R.C., Roig, F., 2013. Chaotic diffusion caused by close encounters with several massive asteroids. II. The regions of (10) Hygiea, (2) Pallas, and (31) Euphrosyne. *Astron. Astrophys.* 550, A85.
- Carruba, V., Huaman, M.E., Domingos, R.C., Santos, C.R.D., Souami, D., 2014. Dynamical evolution of V-type asteroids in the central main belt. *Mon. Not. R. Astron. Soc.* 439, 3168–3179.
- Cellino, A., Zappalà, V., Doressoundiram, A., di Martino, M., Bendjoya, Ph., Dotto, E., Migliorini, F., 2001. The puzzling case of the Nysa–Polana family. *Icarus* 152, 225–237.
- Cellino, A., Bus, S.J., Doressoundiram, A., Lazzaro, D., 2002. Spectroscopic properties of asteroid families. In: Bottke, W.F., Cellino, A., Paolicchi, P., Binzel, R.P. (Eds.), *Asteroids III*. University of Arizona Press, Tucson, pp. 633–643.
- Chesley, S.R. et al., 2014. Orbit and bulk density of the OSIRIS-REX target Asteroid (101955) Benu. *Icarus* 235, 5–22.
- Clark, B.E. et al., 2011. Asteroid (101955) 1999 RQ36: Spectroscopy from 0.4 to 2.4  $\mu$ m and meteorite analogs. *Icarus* 216, 462–475.
- Cotto-Figueroa, D., 2013. Radiation Recoil Effects on the Dynamical Evolution of Asteroids, PhD Dissertation. Ohio University.
- Cotto-Figueroa, D., Statler, T.S., Richardson, D.C., Tanga, P., 2014. Coupled spin and shape evolution of small rubble-pile asteroids: Self-limitation of the YORP effect. *Icarus* (submitted for publication).
- Cuzzi, J.N., Hogan, R.C., Bottke, W.F., 2010. Towards initial mass functions for asteroids and Kuiper Belt Objects. *Icarus* 208, 518–538.
- Delbò, M., Michel, P., 2011. Temperature history and dynamical evolution of (101955) 1999 RQ36: A potential target for sample return from a primitive asteroid. *Astrophys. J.* 728, L42 (5pp).
- Delbò, M., Dell’Oro, A., Harris, A.W., Mottola, S., Mueller, M., 2007. Thermal inertia of near-Earth asteroids and implications for the magnitude of the Yarkovsky effect. *Icarus* 90, 236–249.
- Dell’Oro, A., Cellino, A., 2007. The random walk of Main Belt asteroids: orbital mobility by non-destructive collisions. *Mon. Not. R. Astron. Soc.* 380, 399–416.
- Durda, D.D. et al., 2007. Size-frequency distributions of fragments from SPH/N-body simulations of asteroid impacts: Comparison with observed asteroid families. *Icarus* 186, 498–516.
- Durda, D.D., Bottke, W.F., Enke, B.L., Merline, W.J., Asphaug, E., Richardson, D.C., Leinhardt, Z.M., 2004. The formation of asteroid satellites in large impacts: Results from numerical simulations. *Icarus* 170, 243–257.
- Emery, J.P. et al., 2012. Thermal and Physical Characterization of the OSIRIS-REX Target Asteroid (101955) 1999 RQ36, DPS Contribution No. 102.05.
- Emery, J.P., Fernández, Y.R., Kelley, M.S.P., Warden (née Crane), K.T., Hergenrother, C., Lauretta, D.S., Drake, M.J., Campins, H., Ziffer, J., 2014. Thermal infrared observations and thermophysical characterization of OSIRIS-REX target asteroid (101955) Benu. *Icarus* 234, 17–35.
- Farinella, P., Vokrouhlický, D., Hartmann, W.K., 1998. Meteorite delivery via Yarkovsky orbital drift. *Icarus* 132, 378–387.
- Farnocchia, D., Chesley, S.R., Vokrouhlický, D., Milani, A., Spoto, F., Bottke, W.F., 2013. Near Earth Asteroids with measurable Yarkovsky effect. *Icarus* 224, 1–13.
- Fowler, J.W., Chillemi, J.R., 1992. IRAS asteroid data processing. In: Tedesco, E.F. (Ed.), *The IRAS Minor Planet Survey*, Tech. Report PL-TR-92-2049, Phillips Laboratory, Hanscom Air Force Base, Massachusetts, pp. 17–43.
- Gayon-Markt, J., Delbo, M., Morbidelli, A., Marchi, S., 2012. On the origin of the Almahata Sitta meteorite and 2008 TC<sub>3</sub> asteroid. *Mon. Not. R. Astron. Soc.* 424, 508–518.
- Golubov, O., Krugly, Y.N., 2010. Tangential component of the YORP effect. *Astrophys. J.* 752, L11.
- Hanuš, J. et al., 2011. A study of asteroid pole-latitude distribution based on an extended set of shape models derived by the lightcurve inversion method. *Astron. Astrophys.* 530, A134 (16pp).
- Hanuš, J. et al., 2013. Asteroids’ physical models from combined dense and sparse photometry and scaling of the YORP effect by the observed obliquity distribution. *Astron. Astrophys.* 551, A67 (16pp).
- Hasegawa, S., Müller, T.G., Kawakami, K., Kasuga, T., Wada, T., Ita, Y., Takato, N., Terada, H., Fujiyoshi, T., Abe, M., 2008. Albedo, size, and surface characteristics of Hayabusa-2 sample-return target 162173 1999 JU3 from AKARI and Subaru observations. *Publ. Astron. Soc. Jpn.* 60, 399.
- Ivezić, Ž. et al., 2002. Color confirmation of asteroid families. *Astron. J.* 124, 2943–2948.
- Jacobson, S.A., Scheeres, D.J., 2011. Dynamics of rotationally fissioned asteroids: Source of observed small asteroid systems. *Icarus* 214, 161–178.
- Johansen, A., Oishi, J.S., Mac Low, M.-M., Klahr, H., Henning, T., Youdin, A., 2007. Rapid planetesimal formation in turbulent circumstellar disks. *Nature* 448, 1022–1025.
- Johansen, A., Youdin, A.N., Lithwick, Y., 2012. Adding particle collisions to the formation of asteroids and Kuiper belt objects via streaming instabilities. *Astron. Astrophys.* 537, A125.
- Knežević, Z., Lemaître, A., Milani, A., 2002. The determination of asteroid proper elements. In: *Asteroids III*, pp. 603–612.
- La Spina, A., Paolicchi, P., Kryszczyńska, A., Pravec, P., 2004. Retrograde spins of near-Earth asteroids from the Yarkovsky effect. *Nature* 428, 400–401.
- Lauretta, D.S., et al. The OSIRIS-REX target asteroid 101955 Benu: Constraints on its physical, geological, and dynamical nature from astronomical observations. *Meteorit. Planet. Sci.* (in press).
- Levison, H.F., Duncan, M.J., 1994. The long-term dynamical behavior of short-period comets. *Icarus* 108, 18–36.
- Levison, H.F., Bottke, W.F., Gounelle, M., Morbidelli, A., Nesvorný, D., Tsiganis, K., 2009. Contamination of the asteroid belt by primordial trans-Neptunian objects. *Nature* 460, 364–366.
- Levison, H.F., Duncan, M.J., Thommes, E., 2012. A Lagrangian Integrator for Planetary Accretion and Dynamics (LIPAD). *The Astron. J.* 144, 119.
- Mainzer, A. et al., 2012. Characterizing Subpopulations within the near-Earth Objects with NEOWISE: Preliminary results. *Astrophys. J.* 752, 110.
- Marchi, S. et al., 2012. The violent collisional history of asteroid 4 Vesta. *Science* 336, 690–693.
- Masiero, J. et al., 2011. Main belt asteroids with WISE/NEOWISE I: Preliminary albedos and diameters. *Astrophys. J.* 741, 68 (20pp).
- Masiero, J.R., Mainzer, A.K., Bauer, J.M., Grav, T., Nugent, C.R., Stevenson, R., 2013. Asteroid family identification using the hierarchical clustering method and WISE/NEOWISE physical properties. *Astrophys. J.* 770, 7.
- McSween Jr., H.Y., Ghosh, A., Grimm, R.E., Wilson, L., Young, E.D., 2002. Thermal evolution models of asteroids. In: *Asteroids III*, pp. 559–571.
- Michel, P., Benz, W., Richardson, D.C., 2004. Catastrophic disruption of pre-shattered parent bodies. *Icarus* 168, 420–432.
- Morbidelli, A., Gladman, B.J., 1998. Orbital and temporal distributions of meteorites originating in the asteroid belt. *Meteor. Planet. Sci.* 33, 999–1016.
- Morbidelli, A., Jedicke, R., Bottke, W.F., Michel, P., Tedesco, E.F., 2002. From magnitudes to diameters: The albedo distribution of Near-Earth objects and the Earth collision hazard. *Icarus* 158, 329–342.
- Morbidelli, A., Gounelle, M., Levison, H.F., Bottke, W.F., 2006. Formation of the binary near-Earth object 1996 FG<sub>3</sub>: Can binary NEOs be the source of short-CRE meteorites? *Meteorit. Planet. Sci.* 41, 874–887.
- Morbidelli, A., Bottke, W.F., Nesvorný, D., Levison, H.F., 2009. Asteroids were born big. *Icarus* 204, 558–573.
- Mothé-Diniz, T., Roig, F., Carvano, J.M., 2005. Reanalysis of asteroid families structure through visible spectroscopy. *Icarus* 174, 54–80.
- Mueller, T.G. et al., 2011. Thermo-physical properties of 162173 (1999 JU<sub>3</sub>), a potential flyby and rendezvous target for interplanetary missions. *Astron. Astrophys.* 525, A145 (6pp).
- Mueller, T.G. et al., 2012. Physical properties of OSIRIS-REX target asteroid (101955) 1999 RQ36. Derived from Herschel, VLT/VISIR, and Spitzer observations. *Astron. Astrophys.* 548, A36 (9pp).
- Nesvorný, D., 2012. Nesvorný HCM asteroid families V2.0, NASA Planetary Data System, EAR-A-VARGBDT-5-NESVORNYFAM-V2.0.
- Nesvorný, D., Bottke, W.F., 2004. Detection of the Yarkovsky effect for main-belt asteroids. *Icarus* 170, 324–342.
- Nesvorný, D., Morbidelli, A., 1998. Three-body mean-motion resonances and the chaotic structure of the asteroid belt. *Astron. J.* 116, 3029–3037.
- Nesvorný, D., Vokrouhlický, D., 2006. New candidates for recent asteroid breakups. *Astron. J.* 132, 1950–1958.
- Nesvorný, D., Vokrouhlický, D., 2007. Analytic theory of the YORP effect for near-spherical objects. *Astron. J.* 134, 1750–1768.
- Nesvorný, D., Ferraz-Mello, S., Holman, M., Morbidelli, A., 2002a. Regular and chaotic dynamics in the mean-motion resonances: Implications for the structure and evolution of the asteroid belt. In: Bottke, W.F., Cellino, A., Paolicchi, P., Binzel, R.P. (Eds.), *Asteroids III*. University of Arizona Press, Tucson, pp. 379–394.
- Nesvorný, D., Morbidelli, A., Vokrouhlický, D., Bottke, W.F., Brož, M., 2002b. The Flora family: a case of the dynamically dispersed collisional swarm? *Icarus* 157, 155–172.
- Nesvorný, D., Bottke, W.F., Dones, L., Levison, H.F., 2002c. The recent breakup of an asteroid in the main-belt region. *Nature* 417, 720–722.
- Nesvorný, D., Bottke, W.F., Levison, H., Dones, L., 2003. Recent origin of the solar system dust bands. *Astrophys. J.* 591, 486–497.
- Nesvorný, D., Vokrouhlický, D., Bottke, W.F., 2006a. A main belt asteroid break-up 450 ky ago. *Science* 312, 1490.
- Nesvorný, D., Enke, B.L., Bottke, W.F., Durda, D.D., Asphaug, E., Richardson, D.C., 2006b. Karin cluster formation by asteroid impact. *Icarus* 183, 296–311.
- Nolan, M.C. et al., 2013. Shape model and surface properties of the OSIRIS-REX target Asteroid (101955) Benu from radar and lightcurve observations. *Icarus* 226, 629–640.
- Novaković, B., 2010. Portrait of Theobalda as a young asteroid family. *Mon. Not. Roy. Astron. Soc.* 407, 1477–1486.
- Nugent, C.R., Margot, J.L., Chesley, S.R., Vokrouhlický, D., 2012. Detection of semimajor axis drifts in 54 near-Earth asteroids: New measurements of the Yarkovsky effect. *Astron. J.* 144 (60), 1–13.
- Parker, A., Ivezić, Ž., Jurić, M., Lupton, R., Sekora, M.D., Kowalski, A., 2008. The size distributions of asteroid families in the SDSS Moving Object Catalog 4. *Icarus* 198, 138–155.
- Polishook, D., Broch, N., 2009. Photometry and spin rate distribution of small-sized main belt asteroids. *Icarus* 199, 319–332.
- Pravec, P. et al., 2008. Spin rate distribution of small asteroids. *Icarus* 197, 497–504.

- Pravec, P. et al., 2010. Formation of asteroid pairs by rotational fission. *Nature* 466, 1085–1088.
- Pravec, P., Harris, A.W., 2007. Binary asteroid population. 1. Angular momentum content. *Icarus* 190, 250–259.
- Reddy, V., Corre, L.L., Hicks, M., Lawrence, K., Buratti, B.J., Abell, P.A., Gaffey, M.J., Hardsen, P.S., 2012. Composition of near-Earth Asteroid 2008 EV5: Potential target for robotic and human exploration. *Icarus* 221, 678–681.
- Roig, F., Gil-Hutton, R., 2006. Selecting candidate V-type asteroids from the analysis of the Sloan Digital Sky Survey colors. *Icarus* 183, 411–419.
- Rozitis, B., Green, S.F., 2012. The influence of rough surface thermal-infrared beaming on the Yarkovsky and YORP effect. *Mon. Not. R. Astron. Soc.* 423, 367–388.
- Rubincam, D.P., 2000. Radiative spin-up and spin-down of small asteroids. *Icarus* 148, 2–11.
- Russell, C.T. et al., 2012. Dawn at Vesta: Testing the protoplanetary paradigm. *Science* 336, 684–686.
- Scheeres, D.J., Mirrahimi, S., 2008. Rotational dynamics of a Solar System body under solar radiation torques. *Celest. Mech. Dyn. Astron.* 101, 69–103.
- Scheeres, D.J., Abe, M., Yoshikawa, M., Nakamura, R., Gaskell, R.W., Abell, P.A., 2007. The effect of YORP on Itokawa. *Icarus* 188, 425–429.
- Somers, J.M., Hicks, M.D., Lawrence, K.J., 2008. Optical characterization of planetary radar targets. *Bull. Am. Astron. Soc.* 40, 440.
- Statler, T.S., 2009. Extreme sensitivity of the YORP effect to small-scale topography. *Icarus* 202, 502–513.
- Stuart, J.S., Binzel, R.P., 2004. Bias-corrected population, size distribution, and impact hazard for the near-Earth objects. *Icarus* 170, 295–311.
- Tsiganis, K., Knežević, Z., Varvoglis, H., 2007. Reconstructing the orbital history of the Veritas family. *Icarus* 186, 484–497.
- Vokrouhlický, D., 1998. Diurnal Yarkovsky effect for meter-sized asteroidal fragments' mobility. I. Linear theory. *Astron. Astrophys.* 335, 1093–1100.
- Vokrouhlický, D., 1999. A complete linear model for the Yarkovsky thermal force on spherical asteroid fragments. *Astron. Astrophys.* 344, 362–366.
- Vokrouhlický, D., Čapek, D., 2002. YORP-Induced long-term evolution of the spin state of small Asteroids and Meteoroids: Rubincam's approximation. *Icarus* 159, 449–467.
- Vokrouhlický, D. et al., 2009. Datura family: The 2009 update. *Astron. Astrophys.* 507, 495–504.
- Vokrouhlický, D., Bottke, W.F., 2012. Yarkovsky and YORP effects. In: *Scholarpedia*, vol. 7(5), p. 10599 (the internet open-access encyclopedia).
- Vokrouhlický, D., Nesvorný, D., 2008. Pairs of asteroids probably of common origin. *Astron. J.* 136, 280–290.
- Vokrouhlický, D., Brož, M., Bottke, W.F., Nesvorný, D., Morbidelli, A., 2006a. Yarkovsky/YORP chronology of asteroid families. *Icarus* 182, 118–142.
- Vokrouhlický, D., Brož, M., Bottke, W.F., Nesvorný, D., Morbidelli, A., 2006b. The peculiar case of the Agnia asteroid family. *Icarus* 183, 349–361.
- Vokrouhlický, D., Brož, M., Morbidelli, A., Bottke, W.F., Nesvorný, D., Lazzaro, D., Rivkin, A.S., 2006c. Yarkovsky footprints in the Eos family. *Icarus* 182, 92–117.
- Vokrouhlický, D., Breiter, S., Nesvorný, D., Bottke, W.F., 2007. Generalized YORP evolution: Onset of tumbling and new asymptotic states. *Icarus* 191, 636–650.
- Walsh, K.J., Richardson, D.C., 2006. Binary minor planets. *Annu. Rev. Earth Planet. Sci.* 34, 47–81.
- Walsh, K.J., Richardson, D.C., Michel, P., 2008. Rotational breakup as the origin of small binary asteroids. *Nature* 454, 188–191.
- Walsh, K.J., Morbidelli, A., Raymond, S.N., O'Brien, D.P., Mandell, A.M., 2011. A low mass for Mars from Jupiter's early gas-driven migration. *Nature* 475, 206–209.
- Walsh, K.J., Richardson, D.C., Michel, P., 2012a. Spin-up of rubble-pile asteroids: Disruption, satellite formation, and equilibrium shapes. *Icarus* 220, 514–529.
- Walsh, K.J., Delbó, M., Mueller, M., Binzel, R., De Meo, F.E., 2012b. Physical characterization and origin of binary near-Earth asteroid (175706) 1996 FG<sub>3</sub>. *Astrophys. J.* 748, 104 (7pp).
- Walsh, K.J., Delbó, M., Bottke, W.F., Vokrouhlický, D., Lauretta, D.S., 2013. Introducing the Eulalia and new Polana asteroid families: Re-assessing primitive asteroid families in the inner Main Belt. *Icarus* 225, 283–297.
- Warner, B.D., Harris, A.W., Vokrouhlický, D., Nesvorný, D., Bottke, W.F., 2009. Analysis of the Hungaria asteroid population. *Icarus* 204, 172–182.
- Weidenschilling, S.J., 2011. Initial sizes of planetesimals and accretion of the asteroids. *Icarus* 214, 671–684.
- Zappalà, V., Cellino, A., Farinella, P., Knežević, Z., 1990. Asteroid families. I. Identification by hierarchical clustering and reliability assessment. *Astron. J.* 100, 2030–2046.
- Zappalà, V., Cellino, A., Farinella, P., Milani, A., 1994. Asteroid families. II. Extension to unnumbered multiopposition asteroids. *Astron. J.* 107, 772–801.